energies

MDPI

Review

Lattice-Based Volumetric Heat Sinks for Forced-Convection Cooling of Power Electronics: A Critical Review

Ebelechukwu Okeke, Mehdi Khatamifar and Wenxian Lin *

College of Science and Engineering, James Cook University, Townsville, QLD 4811, Australia; ebelechukwu.okeke@my.jcu.edu.au (E.O.); mehdi.khatamifar2@jcu.edu.au (M.K.)
* Correspondence: wenxian.lin@jcu.edu.au

Abstract

Lattice-based heat sinks have attracted increasing attention as volumetric thermal management architectures for forced-convection cooling of high-power electronic systems. In contrast to conventional plate-fin, pin-fin, and straight-channel configurations, lattice geometries promote three-dimensional flow–solid interaction through interconnected ligament networks that modify boundary-layer development, wake formation, and internal heat-spreading pathways. This review synthesizes recent experimental and numerical studies to examine the thermo-fluid mechanisms governing lattice performance, with emphasis on the coupled influence of porosity, ligament dimensions, topology, orientation, and channel confinement on heat-transfer enhancement and hydraulic resistance. The analysis indicates that while lattice structures can increase average Nusselt number and improve temperature uniformity, these gains are intrinsically linked to pressure-drop penalties associated with flow tortuosity and form drag, resulting in regime-dependent thermal-hydraulic behavior. Apparent discrepancies reported across the literature are frequently attributable to differences in geometric definition, Reynolds-number normalization, and boundary-condition specification rather than to inconsistencies in physical mechanisms. By consolidating geometric scaling, performance metrics, manufacturing considerations, and system-level constraints, this review clarifies the conditions under which lattice heat sinks may provide net benefit relative to conventional cooling technologies and identifies key research directions required to support application-relevant design and evaluation.

Keywords: lattice heat sinks; forced convection; heat transfer; thermal-hydraulic performance; additive manufacturing; power electronics cooling

Check for updates

Academic Editors: Stanislav Boldyryev, Bohong Wang and Timothy Gordon Walmsley

Received: 21 April 2026
Revised: 10 June 2026
Accepted: 12 June 2026
Published: 14 June 2026

Copyright: © 2026 by the authors. Licensee MDPI, Basel, Switzerland. This article is an open access article distributed under the terms and conditions of the Creative Commons Attribution (CC BY) license.

1. Introduction

The rapid expansion of electrification and advanced energy-conversion technologies has driven sustained increases in the power density and functional integration of modern power-electronic systems [1,2], with gravimetric power densities reported up to approximately 10–86 kVA · kg^{-1} in compact converters and traction inverters relevant to automotive and renewable applications [3]. This trend reflects the ongoing drive toward lightweight, high-performance designs. As power densities increase and device packaging becomes increasingly compact, thermal loads within electronic modules intensify [4,5]. Inverter-grade Insulated-Gate Bipolar Transistor (IGBT) modules have been reported to experience local heat fluxes on the order of 100–150 W · cm^{-2} under full-load operation, with future systems expected to approach 500 W · cm^{-2} [6]. Moreover, recent thermal-management optimization studies evaluate boundary heat-flux conditions up

to 300 W · cm^{-2} in high-power drive inverters [7]. These escalating thermal demands increasingly challenge conventional heat-removal strategies.

Thermal management has therefore become a decisive constraint on efficiency, reliability, and service lifetime. Elevated junction temperatures (typically limited to approximately 150 °C for silicon power devices such as Metal-Oxide-Semiconductor Field-Effect Transistor (MOSFETs) and IGBTs, with practical module limits around 175 °C due to packaging C accelerate degradation processes, shift device characteristics, and promote failure mechanisms in MOSFET and IGBT technologies [10,11]. Coupled electrothermal analyses further indicate that temperature-dependent electrical and material properties directly influence system efficiency [12]. Effective heat dissipation is thus a system-level requirement rather than a secondary packaging consideration. In response to increasingly stringent thermal and volumetric constraints, research activity in thermal management has expanded progressively over the past two decades.

Figure 1 illustrates the evolution of Scopus-indexed publications over 2005–2025 on four major cooling architectures: plate- and pin-fin heat sinks, microchannel heat sinks, strut-based lattice heat sinks, and TPMS-based lattice heat sinks, where TPMS is the abbreviation of Triply Periodic Minimal Surface. Conventional extended-surface solutions have maintained sustained research attention, while microchannel cooling experienced accelerated growth during the 2010s. More recently, lattice and additively manufactured (AM) heat sinks have shown pronounced growth, particularly after 2020, indicating increasing interest in architected volumetric cooling strategies.

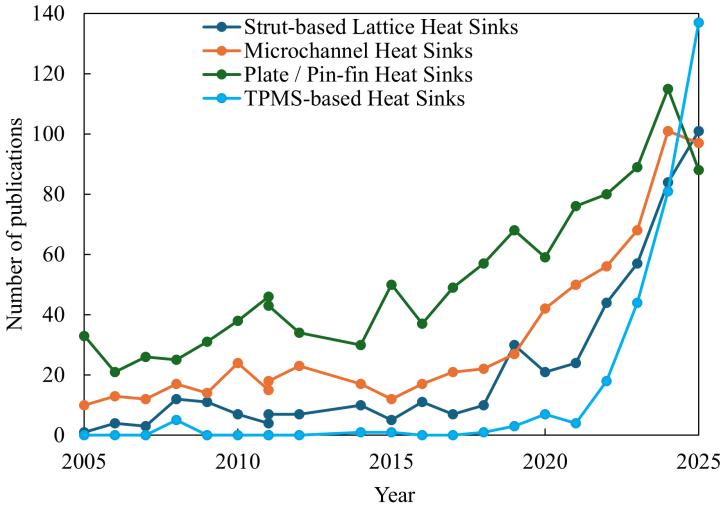


Figure 1. Yearly numbers of Scopus-indexed publications on four major cooling architectures: plate- and pin-fin heat sinks, microchannel heat sinks, strut-based lattice heat sinks, and TPMS-based lattice heat sinks over 2005–2025.

Against this broader research landscape, conventional heat sinks for power electronics are predominantly based on extruded plate fins, pin-fin arrays, or straight microchannels operating under forced convection. Although mature and cost-effective, these configurations are fundamentally governed by boundary-layer development along extended passages and limited three-dimensional flow–surface interaction. Kirchhofer et al. [13] demonstrated that plate-fin heat sinks are dominated by boundary-layer growth along parallel channels. Ismail et al. [14] reported that regular pin-fin arrays exhibit limited transverse mixing and rapidly increasing pressure losses as enhancement is pursued. Similarly, Wu et al. [15] showed that straight microchannel performance is constrained by boundary-layer thickening along smooth walls, motivating geometric modification to improve mixing and heat transfer. More fundamentally, straight microchannel and plate-fin configurations

promote flow predominantly along a single principal direction, with heat transfer governed by streamwise boundary-layer development along streamwise surfaces within parallel flow passages [13,15]. Such channel-dominated architectures inherently limit transverse mixing and restrict three-dimensional thermal interaction within the heat-sink volume [14].

Attempts to intensify heat transfer by increasing surface-area density or reducing hydraulic diameter typically incur substantial hydraulic penalties. Zhang et al. [16] experimentally demonstrated that decreasing microchannel hydraulic diameter increases heat-transfer coefficients but sharply elevates pressure drop and pumping power. Parlak et al. [17] observed similar trends in intensified pin-fin configurations, where enhanced heat-transfer rates were accompanied by significantly higher pressure losses. Numerical optimization by Kamma et al. [18] further showed that geometric modifications aimed at maximizing heat transfer can rapidly shift plate-fin designs into pressure-dominated regimes. These studies collectively illustrate the inherent thermal-hydraulic trade-off that becomes increasingly restrictive as compactness requirements tighten and allowable auxiliary cooling power is limited.

To address these architectural constraints, lattice heat sinks have emerged as an alternative class of volumetric cooling structures. In the context of thermal management, lattice heat sinks refer to architected porous structures composed of interconnected ligament networks that generate three-dimensional internal flow pathways [19]. Unlike channel-based configurations, lattice architectures distribute coolant through interconnected volumetric pathways, enabling heat exchange throughout the internal volume rather than primarily along external fin surfaces [20]. Recent advances in additive manufacturing (AM) have enabled fabrication of complex three-dimensional lattice architectures that are impractical using conventional subtractive or casting-based manufacturing methods, particularly when precise control of relative density, pore topology, and permeability is required. Du Plessis et al. [21] emphasized that layer-by-layer fabrication permits internal ligament networks with geometric freedoms unattainable through traditional manufacturing. In thermal applications, lattice structures operate as volumetric heat-transfer media in which flow and heat exchange develop within interconnected passages rather than predominantly along external fin surfaces [22–24]. Under turbulent forced convection conditions (Re $\approx$ 5000–45,000) [19], architectured lattices, including strut-based lattices and Triply Periodic Minimal Surface (TPMS), enhance convective transport through fundamentally different mechanisms. Strut-based lattices promote mixing through repeated boundary-layer disruption, flow separation, and wake interaction around discrete ligaments, whereas TPMS architectures, characterized by continuous surfaces and interconnected channels, facilitate more distributed, shear-driven mixing via flow splitting and recombination. Large-eddy simulations by Corbett and Thole [25] resolved ligament-scale separation and vortex structures associated with this process, while conjugate heat-transfer simulations by Kaur et al. [26] demonstrated that the continuous solid ligament network enhances internal heat spreading and solid–fluid coupling. Together, these mechanisms enable enhanced heat-transfer performance and improved thermal uniformity within compact volumes, albeit often accompanied by increased pressure drop and pumping power requirements. Vaglio et al. [27] experimentally showed that enhanced convective transport in Laser Powder Bed Fusion (LPBF) Body-Centered-Cubic (BCC) lattices is accompanied by substantial pressure-drop penalties arising from strut-induced separation and form drag. Padrão et al. [20] numerically reported that geometric features intensifying mixing also increase flow tortuosity and inertial losses, leading to rapid pressure-drop escalation. Batikh et al. [28] further demonstrated that under transitional-to-turbulent forced convection conditions (Re $\approx$ 1400–14,200), lattice configurations outperform straight-fin or pin-fin

baselines only within specific operating regimes once pressure-drop and pumping power constraints are incorporated.

Accordingly, maximizing Nusselt number alone is insufficient for design evaluation. Comparative thermo-hydraulic studies show that configurations ranked favorably by heat-transfer metrics may underperform once pressure drop is accounted for [22,29]. Balanced performance metrics that integrate both heat-transfer enhancement and hydraulic expenditure are therefore essential for rational, application-oriented designs.

Although several reviews have examined additively manufactured lattices and TPMS structures for heat-transfer applications, including those by Kaur et al. [26], Sajjad et al. [30], Amara et al. [31], Wang et al. [32], Ifa et al., [33], and Al-Safadi [34], etc., as summarized in Table 1, most existing syntheses focus on geometric taxonomy, manufacturing considerations, topology-specific performance, or isolated heat-transfer enhancement trends. In particular, TPMS and strut-based lattices are often treated either independently or compared using inconsistent normalization frameworks. As a result, systematic comparisons that account for Reynolds-number scaling, pressure-drop constraints, and regime-dependent thermo-hydraulic performance remain limited. A unified framework that consistently evaluates both discrete-ligament and continuous-surface architectures under forced convection is therefore still lacking.

As summarized in Table 1, prior reviews provide valuable insights into lattice fabrication strategies and topology-specific performance trends; however, a unified, normalization-consistent thermo-hydraulic framework for forced-convection lattice heat sinks remains underdeveloped.

The present review addresses these gaps by establishing a unified thermo-fluid framework for forced-convection lattice heat sinks that consistently evaluates both strut-based and TPMS-based architectures under common scaling and performance metrics. Lattice heat sinks are explicitly framed as regime-dependent thermo-fluid systems, in which heat-transfer enhancement and hydraulic resistance emerge from coupled interactions among geometry, flow development, and solid conduction. Emphasis is placed on identifying dominant transport mechanisms, reconciling conflicting trends across experimental and numerical studies, and evaluating performance using integrated thermal–hydraulic metrics under consistent Reynolds-number definitions

The quantitative contribution of this review is threefold. First, it consolidates the normalization problem by explicitly comparing the characteristic-length, Reynolds-number, Nusselt-number, friction-factor, and pumping power definitions used across the surveyed literature. Second, it introduces a benchmarking-envelope approach in which reported thermal gains and hydraulic penalties are grouped according to their original comparison basis, including equal Reynolds number, equal pumping power, similar pressure drop, or comparison against a conventional fin, microchannel, zigzag, or printed-circuit baseline. Third, it summarizes representative order-of-magnitude ranges of thermal enhancement and hydraulic penalty in Section 5.4, rather than relying only on qualitative statements or isolated (Nu)-enhancement claims. In this way, the review does not propose a universal correlation across incompatible datasets, but provides a quantitative framework for interpreting reported performance ranges without over-normalizing studies that use different geometries, baselines, fluids, and boundary conditions.

Table 1. Scope comparison of representative reviews related to lattice-based thermal management. Note: LS = Lattice Structure, TPMS = Triply Periodic Minimal Surface, AM = Additive Manufacturing, TH = Thermal-Hydraulic, Re = Reynolds number.

Review (Year)	Main Scope/Emphasis	LS	TPMS	AM	Forced Convection	TH Trade-Off	Re/Scaling Consistency
Kaur et al. (2021) [35]	AM lattice structures for thermal/heat-exchanger applications	Yes	No	Yes	Partial	Partial	Limited
Sajjad et al. (2022) [30]	Manufacturing and applications of lattice structures in thermal systems	Yes	Partial	Yes	Partial	Partial	Limited
Yan et al. (2023) [36]	Comparative review on turbulent convection in 3D truss/ cellular structures	Yes	No	Limited	Yes	Yes	Limited
Amara et al. (2025) [31]	Review of TPMS structures for cooling heat sinks	No	Yes	Partial	Yes	Yes	Limited
Wang et al. (2025) [32]	Comprehensive review of TPMS structures for thermal management	Partial	Yes	Partial	Partial	Yes	Limited
Dharmalingam et al. (2022) [37]	TPMS-based heat exchanger designs and thermal-hydraulic performance	No	Yes	Yes	Yes	Yes	Limited
Ifa et al. (2026) [33]	TPMS-enabled architectures for heat dissipation in thermal systems	No	Yes	Partial	Partial	Partial	Limited
Yeranee and Rao (2022) [38]	Flow and heat transfer in TPMS-based cooling channels	Yes	Yes	Partial	Yes	Partial	Limited
Rashid et al. (2025) [39]	TPMS structures for heat sinks, heat exchangers, and PCM-based thermal management	No	Yes	Yes	Yes	Yes	Limited
Al-Safadi et al. (2026) [34]	Quantitative synthesis/correlations for TPMS heat transfer and friction	Partial	Yes	Limited	Yes	Yes	Yes
This review	Forced-convection lattice heat sinks with regime-aware comparison and consistent metrics	Yes	Yes	Yes	Yes	Yes	Yes

2. Thermally Relevant Classification of Lattice Structures

Lattice structures employed as heat sinks encompass a wide range of geometric configurations, unit-cell topologies, and connectivity patterns. Although many classification schemes originate from structural mechanics or manufacturability considerations, not all geometric distinctions are equally meaningful from a heat-transfer perspective. To provide a visual overview of the representative lattice structures considered in this review, Figure 2 illustrates commonly used strut-based and TPMS-based lattice structures for thermal management applications. The commonly used strut-based lattice structures include BCC (Body-Centered-Cubic), FCC (Face-Centered-Cubic), Octet-truss, Pyramidal, Kelvin cell, Cubic, X-Type, and Tetraheron, while the commonly used TPMS-based lattice structures include Gyroid, Fischer–Koch S (FKS), Diamond, Primitive, Lidinoid, IWP (I-graph-Wrapped Package), Neovius, and Schwarz, although there are some other lattice structures used as well, as summarized, e.g., in [36,40,41]. The mathematical representations of such TPMS structures [33,41] are presented in Appendix A.

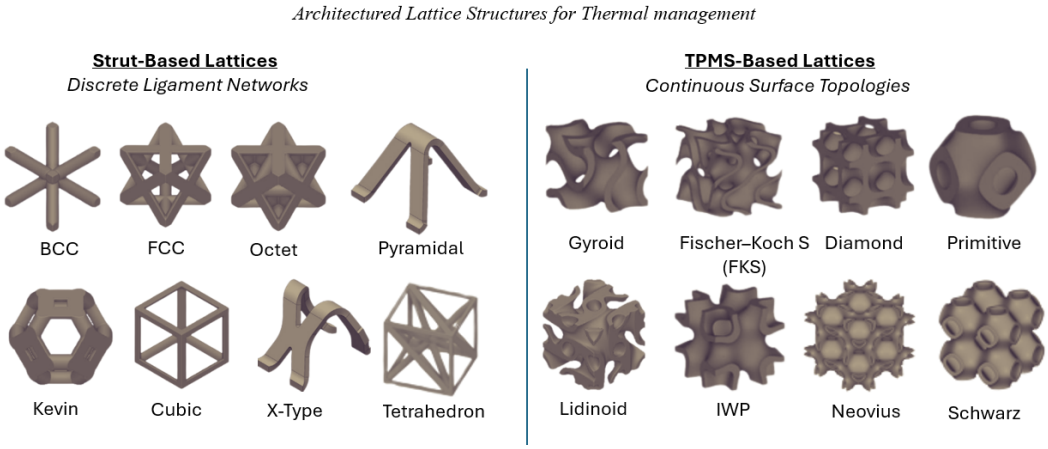


Figure 2. Schematic of the commonly used lattice structures for thermal management applications: strut-based lattice structures (**left column**) and TPMS-based lattice structures (**right column**) (after [36,40,41]).

2.1. Thermo-Fluid-Oriented Classification Framework

Under forced-convection conditions relevant to power electronics, thermal performance is governed by the interplay between internal flow development, surface-area exposure, solid heat-spreading pathways, and hydraulic resistance.

Existing reviews on lattice structure heat sinks have primarily focused on geometric taxonomy, manufacturing considerations, or topology-specific performance trends, without systematically organizing lattice structures based on their coupled thermo-fluid transport characteristics under forced convection. While individual studies report boundary-layer disruption, wake interaction, and conduction effects, these mechanisms are typically discussed in isolation.

The qualitative rankings in Table 2 synthesize recurring thermo-fluid tendencies reported across recent experimental and numerical studies of strut-based and TPMS-based heat sinks. Strut-based lattices with higher obstruction commonly intensify boundary-layer renewal and wake-driven mixing, but exhibit stronger form-drag and Forchheimer-type pressure-loss penalties, as shown for Octet-truss and BCC configurations and related periodic arrays [42–47]. In contrast, TPMS-based topologies provide continuous surfaces and are frequently reported to yield smoother flow development and competitive thermal-hydraulic performance, although the relative advantage depends on porosity, orientation, and operating regime [34,48–52]. Flow-guiding or semi-closed insert concepts can improve surface utilization and temperature uniformity by redistributing coolant, typically at the

expense of increased pressure drop [53–56]. In this context, conduction connectivity reflects the role of solid-network continuity and architecture-dependent effective conduction pathways, which vary with relative density and topology [57,58].

The trends summarized in Table 2 are consistent with the conceptual framework illustrated in Figure 3, which maps mixing intensity and pressure-drop penalty across lattice architectures.

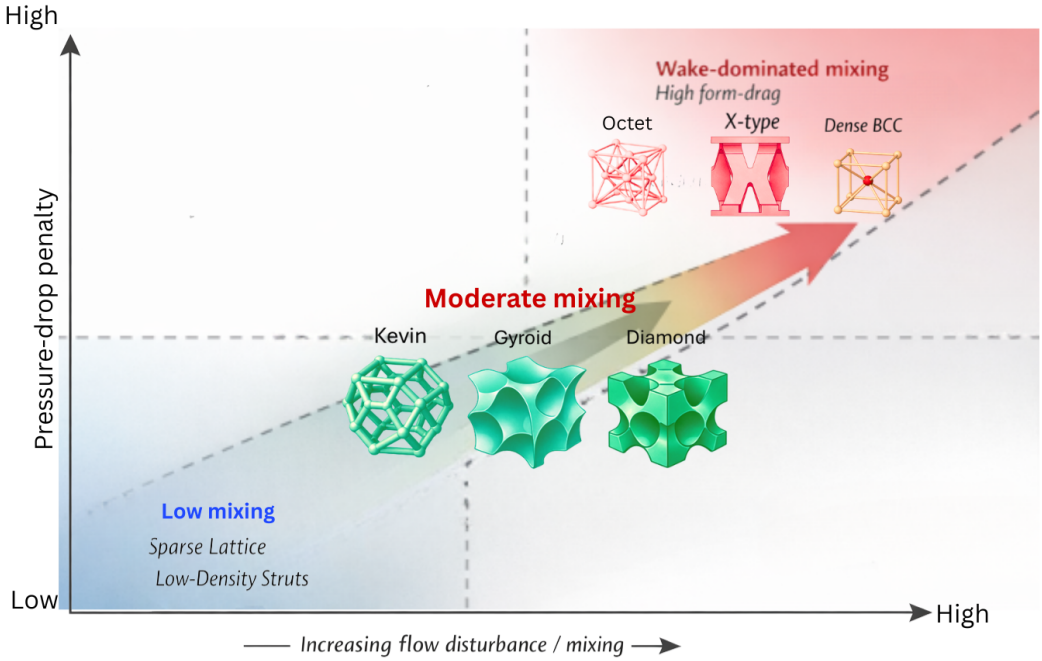


Figure 3. Thermo-fluid classification of lattice structures based on mixing and pressure-drop penalty.

Table 2. Qualitative thermo-fluid tendencies of lattice structure classes under steady forced convection (rankings are qualitative and regime-dependent; ordering may shift with Reynolds number, porosity, orientation, and confinement).

Structure Class	Typical Flow Features	Mixing	Form Drag (Δp Sensitivity)	Conduction Connectivity	Favorable When	Ref.
TPMS-based (Gyroid, Diamond, Schwarz, etc.)	Continuous surfaces; smoother flow paths.	Medium	Low–Medium	Medium (density-dependent)	Δp budget limited; uniformity prioritized.	[59–61]
Strut-based, open/ low obstruction	Larger pores; partial boundary-layer renewal.	Low–Medium	Low–Medium	Medium	Low Δp with moderate enhancement.	[62]
Strut-based, dense/ high obstruction	Strong boundary-layer interruption; wake interaction.	High	High	High (increase with density/ connectivity)	Maximum heat-transfer gain acceptable with higher Δp.	[45,57,63]
Flow-guiding/ semi-closed	Directed jets; reduced bypass; wall interaction.	High (localized)	High	Medium–High (design-dependent)	Hot-spot mitigation; tuned to fan/pump limits.	[58,61,64]
Stretch-dominated (e.g., Octet-truss)	High nodal connectivity; continuous solid paths.	Medium–High	Medium–High	High (connectivity-driven)	Conjugate heat spreading important.	[51]
Bending-dominated (e.g., Kelvin-type)	Lower connectivity; smoother passages.	Medium	Medium	Medium–Low (topology-dependent)	Δp and uniformity prioritized over peak Nu.	[65,66]

Strut-based lattices consist of discrete cylindrical or prismatic ligaments connected at nodes, creating localized geometric discontinuities and curvature variations [67]. Under forced convection, such features promote repeated flow redirection and boundary-layer interruption, leading to enhanced convective heat-transfer. Qian et al. [68] experimentally and numerically demonstrated that a BCC topology can achieve approximately 35% higher Nusselt numbers compared to conventional finned and foam-based heat sinks. This was observed under jet impingement conditions corresponding to inlet velocities of 1–4 m/s and a representative operating condition of the dimensionless pump power $C_f \mathrm{Re}^3 \approx 8.45 \times 10^{12}$ (where C_f is friction coefficient). This enhancement is commonly attributed to increased flow disturbance and secondary flow structures induced by ligament interactions. However,

these same characteristics also introduce form-drag-dominated resistance, particularly at moderate to high Reynolds numbers [27,69]. As a result, strut-based structures often exhibit pronounced heat-transfer enhancement accompanied by significant hydraulic penalties.

In contrast, TPMS-based lattices are characterized by smooth, continuous surfaces with gradually varying curvature and no discrete node junctions [48,49]. This geometric continuity tends to promote more uniform flow development compared with discrete-ligament networks [50]. Quantitative comparisons by Richard et al. [51] showed that, at comparable porosity ($\varepsilon \approx 0.79$) and Reynolds numbers over Re ≈ 22–48, Gyroid TPMS structures exhibit lower pressure drop than Kelvin-type lattices (≈3% reduction at 9 m/s), and substantially lower pressure drop than BCC structures (up to 47% reduction under comparable conditions). However, the smoother topology of TPMS structures promotes more continuous flow development with reduced abrupt flow disturbances compared to discrete-ligament lattices, with fluid transport occurring through interconnected channels that facilitate flow redistribution and complex flow pathways [70,71]. As a result, TPMS structures may exhibit lower peak convective enhancement than dense strut-based configurations under certain conditions, but can provide more uniform thermal fields and favorable thermo-hydraulic performance depending on topology, porosity, and Reynolds number. This highlights that TPMS-based systems also exhibit a trade-off between enhanced mixing and increased viscous and inertial losses. Experimental and numerical investigations have shown that topology-optimized TPMS channels can enhance Nusselt number by up to 70–80%, while simultaneously reducing or increasing pressure drop depending on flow redistribution and design strategy [60,72].

2.2. Stretch-Dominated and Bending-Dominated Architectures: Thermal Implications

Within this thermo-fluid framework, lattice architectures can be further interpreted through established mechanical classifications, such as stretch-dominated and bending-dominated topologies, which influence conduction pathways and thermal transport behavior [73].

Stretch-dominated architectures typically exhibit higher nodal connectivity and more continuous axial load paths. From a thermal perspective, this connectivity can provide relatively direct solid conduction routes between the heated base and the lattice interior, potentially improving heat spreading within the solid framework [74].

Bending-dominated lattices, in contrast, generally possess lower nodal connectivity and more compliant beam-like frameworks [75]. While such geometries may provide higher specific surface area or intensified local flow interaction, their conduction pathways may be less continuous, influencing internal temperature redistribution.

Pelanconi et al. [76] compared lattice cores for compact heat exchangers and demonstrated that thermal performance depends not only on surface area and pressure drop but also on effective solid thermal conductivity. Their results show that increased surface interaction does not automatically guarantee improved global heat spreading. Under forced convection, this can lead to configurations with strong local heat-transfer coefficients but limited improvement in overall temperature uniformity [77].

Thus, mechanical classification alone does not determine thermal-hydraulic behavior; its relevance must be interpreted alongside flow development characteristics and solid–fluid coupling.

2.3. Open, Semi-Closed, and Flow-Guiding Lattice Configurations

Another key thermo-fluid distinction arises from the degree of flow confinement and guidance imposed by lattice architecture

Open lattice configurations provide relatively unobstructed flow passages with larger effective pore sizes. This typically reduces hydraulic resistance but also decreases surface-area-to-volume ratio and fluid–solid interaction intensity. Ho et al. [62] showed that increasing unit-cell size in additively manufactured lattices reduces both pressure drop and convective heat-transfer enhancement. Similarly, Richard et al. [51] evaluated Kelvin, BCC, and Gyroid structures at comparable porosities and demonstrated that higher-porosity configurations exhibit lower hydraulic resistance but reduced heat-transfer intensity. Complementary simulations by Tang et al. [52] reported similar trends for TPMS lattices, where enlarging through-flow passages lowered pressure drop while reducing Nusselt number. Collectively, these studies indicate that more open architectures tend to reduce hydraulic penalties at the expense of diminished volumetric heat-transfer augmentation.

Semi-closed configurations, by contrast, impose greater internal flow constraint, increasing fluid–surface interaction and promoting cross-stream transport. Yan et al. [78] demonstrated that inserting X-lattice cores into honeycomb channels induces secondary vortices that enhance wall heat transfer but substantially increase pressure drop. Aider et al. [23] and Lorenzon et al. [43] similarly reported that more obstructed lattice topologies generate higher Nusselt numbers while incurring elevated form-drag-induced losses. High-fidelity simulations by Shi et al. [67] further confirmed that intensified vortex interaction enhances convective transport but increases friction factor. These findings consistently show that increased flow confinement strengthens convective augmentation but amplifies hydraulic resistance.

More recently, flow-guiding lattice designs have been proposed to redistribute coolant toward high-heat-flux regions or reduce bypass flow near channel walls [54–56]. From a thermo-fluid standpoint, such architectures can improve surface utilization efficiency and temperature uniformity. However, deliberate flow redirection generally increases pressure drop, reinforcing that geometric complexity alone does not guarantee net performance improvement.

2.4. Implications for Comparative Assessment and Design

The classifications discussed above demonstrate that no single lattice architecture is intrinsically optimal for forced-convection heat-sink applications. Thermal-hydraulic performance emerges from the coupled interplay among surface exposure, internal flow development, solid heat spreading, and hydraulic resistance.

Meaningful comparison across studies therefore requires consistent thermo-fluid framing rather than reliance on isolated geometric descriptors. By grouping architectures according to dominant heat-transfer and flow characteristics, apparent inconsistencies in reported Nusselt-number enhancement and pressure-drop behavior can be interpreted more systematically.

This thermally oriented classification provides a unified conceptual foundation for subsequent analysis of geometric parameters and performance trends. It establishes that lattice heat-sink performance is fundamentally governed by coupled thermo-fluid mechanisms rather than topology alone, and that apparent discrepancies in reported trends can be systematically interpreted through differences in flow development, surface interaction, and hydraulic resistance across architectures and operating regimes.

3. Thermo-Hydraulic Mechanisms in Lattice Heat Sinks

Lattice-based heat sinks operate as volumetric forced-convection thermal-management systems in which heat transfer and hydraulic resistance are governed by coupled fluid flow, solid conduction, and fluid–solid interfacial convection. Unlike conventional plate-fin or pin-fin heat sinks, where the coolant interacts mainly with external extended surfaces,

lattice and TPMS architectures distribute heat-transfer surfaces throughout the flow volume. This produces repeated boundary-layer interruption, local acceleration and deceleration, secondary-flow generation, wake interaction, and three-dimensional solid heat spreading. Therefore, their performance cannot be evaluated only by heat-transfer enhancement; it must be interpreted through the coupled balance between convective augmentation and pressure-drop penalty [30,32,34,38,69]. The dominant thermo-hydraulic mechanisms are illustrated schematically in Figure 4.

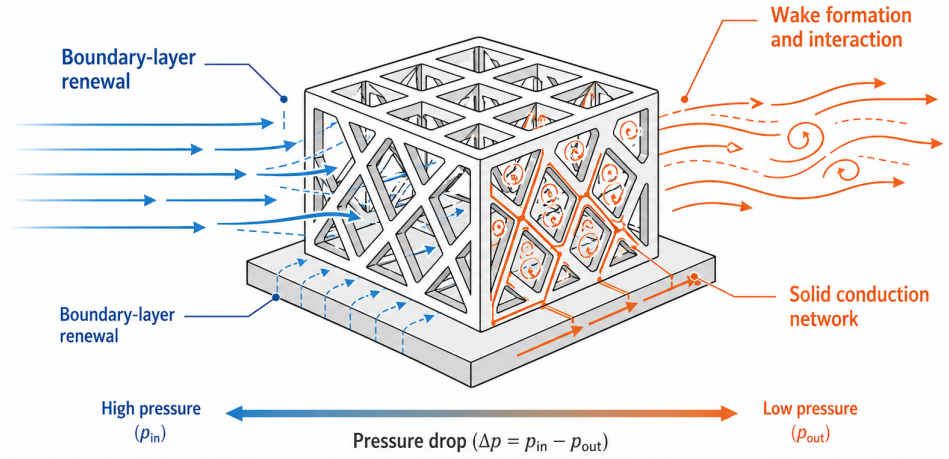


Figure 4. Schematic illustration of dominant thermo-fluid mechanisms in lattice heat sinks under forced convection.

3.1. Governing Transport Framework

The underlying physics of lattice heat sinks can be described using the governing equations for steady, incompressible, single-phase forced convection in the fluid region, coupled with heat conduction in the solid lattice. For the fluid domain, the continuity, momentum, and energy equations are generally written as

$$\nabla \cdot \mathbf{u} = 0, \tag{1}$$

$$\rho_f(\mathbf{u} \cdot \nabla)\mathbf{u} = -\nabla p + \mu_f \nabla^2 \mathbf{u}, \tag{2}$$

$$\rho_f c_{p,f}(\mathbf{u} \cdot \nabla T_f) = k_f \nabla^2 T_f, \tag{3}$$

where $\mathbf{u}$, p, T_f, ρ_f, μ_f, $c_{p,f}$, and k_f are the velocity vector, pressure, fluid temperature, fluid density, dynamic viscosity, specific heat, and fluid thermal conductivity, respectively. In the solid lattice, heat transfer is governed by conduction:

$$\nabla \cdot (k_s \nabla T_s) = 0, \tag{4}$$

where T_s and k_s are the solid temperature and solid thermal conductivity. At the fluid–solid interface, conjugate heat transfer requires both temperature continuity and heat-flux continuity:

$$T_f = T_s, \tag{5}$$

$$-k_f \frac{\partial T_f}{\partial n} = -k_s \frac{\partial T_s}{\partial n}. \tag{6}$$

The governing equations and interface conditions in Equations (1)–(6) show that the performance of lattice heat sinks is not controlled by surface area alone. The heat-transfer rate depends on how the lattice geometry modifies both the fluid-side transport and the solid-side conduction pathway. In discrete strut-based lattices, the ligament diameter, ligament orientation, node connectivity, and unit-cell arrangement control wake forma-

tion, local impingement, flow separation, and conduction through the solid frame. In TPMS lattices, the continuous curvature, wall thickness, level-set parameter, and channel connectivity control the distribution of flow pathways, interfacial area, and solid heat-spreading resistance [32,34,38].

3.2. Dimensionless Interpretation of the Mechanisms

The mechanisms described above are commonly interpreted using dimensionless thermal and hydraulic parameters, including the Reynolds number (Re), hydraulic diameter (D_h), Nusselt number (Nu), friction factor (f), pressure drop (Δp), pumping power (P_{pump}), and thermo-hydraulic performance factor (η). In the present section, these quantities are introduced only as interpretive links between geometry and physics: Re identifies the relative importance of inertial and viscous effects, Nu represents convective heat-transfer enhancement, f and Δp represent hydraulic penalty, and P_{pump} and η connect thermal gain with flow-driving cost. Detailed definitions, normalization choices, and benchmarking implications are discussed later in Section 5.

This separation avoids interpreting heat-transfer enhancement in isolation. For example, the same geometric features that increase Nu, such as surface-area density, boundary-layer renewal, and vortex-assisted mixing, can also increase f, Δp, and pumping power. Therefore, the mechanisms discussed in this section should be interpreted together with the performance metrics, scaling definitions, and benchmarking framework presented in Section 5.

3.3. Solid Conduction and Conjugate Heat-Transfer Pathways

A defining feature of lattice heat sinks is the continuous solid network extending from the heated base into the flow domain. Heat is first conducted through the solid ligaments or TPMS walls and is then transferred convectively from the wetted surfaces to the coolant. This distributed conduction–convection pathway distinguishes lattice heat sinks from conventional fins and requires conjugate heat-transfer interpretation [26,74,79].

Conjugate simulations by Kaur and Singh [26] demonstrated that heat propagates through interconnected ligaments into the interior of octet-based structures, shaping interfacial temperature distributions and strengthening conduction–convection coupling. Comparative analysis across unit-cell topologies further showed that higher ligament connectivity significantly alters thermal-transport behavior relative to simpler frameworks [80]. Son et al. [74] confirmed experimentally and numerically that overall performance depends on ligament conduction resistance and surface efficiency, governed by cross-sectional geometry and material conductivity. Similarly, Kemerli and Kahveci [81] showed that variations in strut length and diameter simultaneously modify pressure drop and heat transfer, including at fixed pumping power, highlighting the dominant role of geometry.

The relative importance of solid conduction and fluid convection changes with Reynolds number and material conductivity [82]. At low flow rates, solid conduction pathways and contact with the heated base can strongly influence temperature uniformity and surface utilization. As the Reynolds number increases, thinner thermal boundary layers increase the fluid-side heat-transfer coefficient, and the dominant thermal resistance may shift toward interfacial convection or hydraulic limitation. Shahrzadi et al. [83] showed that, for Reynolds numbers of approximately 1–150, the role of solid conductivity becomes less dominant as forced convection intensifies. Lattice heat sinks are therefore best described as conjugate heat-transfer systems in which solid conduction and fluid convection are intrinsically coupled rather than independently optimized. Thus, solid conduction is most likely to predominate when k_s is low, ligament or wall thickness is small, porosity is high, conduction pathways from the heated base are long or poorly connected, or the imposed

heat flux is spatially non-uniform; fluid-side convection becomes more limiting when the solid lattice is highly conductive and well connected but the coolant-side heat-transfer coefficient remains low.

3.4. Boundary-Layer Renewal and Local Convective Enhancement

Under forced convection, the coolant repeatedly encounters ligaments, struts, nodes, or curved TPMS walls. This interaction causes local boundary-layer formation, disruption, and redevelopment. Thin hydrodynamic and thermal boundary layers near leading edges or high-curvature regions produce locally elevated heat-transfer coefficients [25,79,80,84]. Successive lattice elements interrupt the continuous boundary-layer growth that would otherwise occur in straight channels or simple fin arrays, thereby improving local convective transport [53,78].

The effectiveness of boundary-layer renewal depends on ligament spacing, wall thickness, unit-cell size, porosity, surface curvature, topology, and Reynolds number. Padrão et al. [20] demonstrated that, in TPMS lattices operating in a laminar regime of approximately Re = 3–60, internal geometry determines how effectively thermal energy is transported through the fluid volume and how pressure losses develop along the structure. Ho et al. [85] similarly showed that variations in ligament diameter and unit-cell geometry simultaneously modify Nusselt number and pressure drop. These results confirm that lattice performance is governed by geometry-controlled flow development rather than by surface-area increase alone.

3.5. Vortex Generation, Flow Mixing, and Thermal Uniformity

Flow separation at ligament leading edges, strut intersections, or curved TPMS passages generates wake-like vortical structures that interact with downstream elements and promote cross-stream transport. Shi et al. [86] identified composite vortex systems, including horseshoe vortices and downstream wake structures, in BCC lattices. Wang et al. [87] demonstrated that lattice-induced vortices increase turbulent kinetic energy and that pitch governs vortex strength. Park et al. [24] linked improved performance of pyramidal and tetrahedral cores to increased internal velocity and turbulence levels. Wake-induced mixing transports heated fluid away from solid surfaces and replenishes thermal boundary layers with cooler fluid, thereby increasing convective heat transfer [88,89].

Enhanced mixing can also improve temperature uniformity by reducing thermal stratification and suppressing localized hot spots. Lee et al. [90] numerically optimized a BCC lattice heat sink for temperature uniformity and demonstrated substantial reductions in spatial temperature variation due to internal flow redistribution. This temperature-uniformity benefit is particularly important for power-electronics cooling, where thermal gradients can reduce reliability even when the average heat-transfer coefficient is high [91,92].

3.6. Hydraulic Penalty, Tortuosity, and Form Drag

The same geometric mechanisms responsible for heat-transfer enhancement also generate hydraulic penalties. Vortex formation, flow separation, local contraction and expansion, repeated flow redirection, and increased wetted surface area all contribute to pressure loss. Chaudhari et al. [42] showed that pressure loss in octet-truss lattices follows Forchheimer-type behavior, with inertial contributions becoming increasingly important at higher Reynolds numbers. Lorenzon et al. [43] similarly reported that configurations producing stronger convective enhancement incur markedly higher pressure losses, and that inertial penalties intensify with increasing Reynolds number.

In addition to wake-induced drag, lattice geometries inherently increase flow tortuosity. Three-dimensional acceleration, deceleration, and directional change generate pressure losses associated with wall shear, form drag, and momentum exchange. Experimental

and numerical studies consistently show that the pressure drop of lattice heat sinks can increase more rapidly with Reynolds number than that of streamlined fins or straight channels [42,43,69]. Therefore, elevated (Nu) values should not be interpreted as evidence of superior heat-sink performance unless (f), (ΔP), P_{pump}, or (η) are evaluated simultaneously.

3.7. Mechanistic Interpretation for Design

Consequently, the net thermo-hydraulic performance of a lattice heat sink reflects the balance between convective heat-transfer enhancement and hydraulic penalty rather than any single mechanism acting in isolation. Surface-area density, boundary-layer renewal, vortex generation, and solid conduction pathways can all increase heat-transfer rate, but they may simultaneously increase friction factor and pumping power. This explains why different studies sometimes report apparently conflicting rankings for BCC, octet, X-lattice, Gyroid, Diamond, Primitive, and other TPMS or strut-based architectures: the ranking depends on Reynolds number, porosity, wall thickness, characteristic-length definition, boundary condition, and whether the comparison is made at equal flow rate, equal Reynolds number, equal pressure drop, or equal pumping power [32,34,38,69].

A mechanistic interpretation therefore requires the following sequence: lattice topology and geometric scale define (D_h), (ε), (A_s / V_c), tortuosity, and solid conduction pathways; these parameters determine boundary-layer renewal, vortex generation, local acceleration, and pressure loss; the resulting thermal and hydraulic responses are then quantified using (Nu), (f), (ΔP), (PP), (Q/PP), and (η). This framework provides a quantitative basis for interpreting the literature and for guiding application-oriented lattice heat-sink design.

4. Effect of Geometric Parameters on Forced-Convection Performance of Lattice Heat Sinks

The forced-convection performance of lattice-based heat sinks is governed by geometric parameters that control surface-area density, internal flow development, solid–fluid coupling, and hydraulic resistance. Unlike conventional finned heat sinks, typically characterized by a limited set of independent variables, lattice architectures introduce multiple interdependent descriptors, including ligament diameter, unit-cell topology, porosity, and orientation, whose influences are inherently coupled. These geometric descriptors apply to both discrete-ligament (strut-based) lattices and continuous-surface TPMS architectures, although their physical interpretation differs due to distinct flow pathways and solid–fluid interaction mechanisms.

Consequently, trends reported across the literature often reflect geometry-flow interactions rather than fundamental contradictions. Variations in Reynolds number, porosity, and unit-cell configuration shift the balance between heat-transfer enhancement and pressure-drop penalty (ΔP), repositioning a design within the conceptual thermal-hydraulic envelope illustrated in Figure 4. This section therefore examines the governing geometric parameters with emphasis on physically consistent mechanisms rather than isolated performance metrics.

4.1. Porosity and Relative Density

Porosity is among the most frequently reported geometric parameters in lattice heat-sink studies and is commonly used as a primary basis for comparison. Increasing porosity generally enhances flow permeability and reduces hydraulic resistance, whereas decreasing porosity increases solid volume fraction and surface-area density. Ali and Sen [93] performed coupled FE-CFD simulations on Gyroid and lattice-based architectures with porosities of 65–90%, showing monotonic increases in permeability and corresponding reductions in pressure drop as interconnected flow pathways enlarged. Timercan et al. [94]

fabricated diamond and Gyroid lattices at 60–80% porosity and similarly reported higher intrinsic permeability at higher porosity, with lower porosity increasing solid fraction and hydraulic resistance. Egan et al. [95] further demonstrated approximate power-law scaling between permeability and porosity over the 60–90% ranges. Collectively, these studies consistently indicate that increasing porosity enhances bulk flow transport through improved void connectivity and reduced hydraulic resistance.

Importantly, similar porosity-dependent trends have been consistently observed in TPMS-based structures, although the underlying mechanisms differ due to their continuous-surface topology. In TPMS lattices, increasing porosity enlarges interconnected flow channels and reduces flow resistance, while simultaneously decreasing surface-area density and fluid–solid interaction intensity [96,97]. However, unlike discrete strut-based lattices, the effect of porosity in TPMS lattices is strongly coupled with topology-dependent tortuosity and channel curvature, which influence flow redistribution and mixing behavior beyond simple permeability scaling [97].

Nevertheless, porosity alone does not uniquely dictate forced-convection performance. Liang et al. [44] tested FCC lattices with identical porosity (0.92) but different ligament cross-sectional shapes, reporting heat-transfer differences of 25–31% and distinct pressure-drop responses at the same Reynolds number. Similarly, Aider et al. [23] compared multiple lattice topologies at porosity ≈0.88 and observed heat-transfer coefficients spanning 167–415 $W \cdot m^{-2} \cdot K^{-1}$, accompanied by substantial variation in hydraulic penalty. These findings demonstrate that topology and ligament arrangement critically influence convective behavior even when porosity is fixed.

This limitation is particularly evident in TPMS structures, where different topologies at identical porosity can exhibit substantially different thermo-hydraulic behavior. Comparative studies of Gyroid, primitive, and IWP structures demonstrate that variations in surface curvature and channel connectivity lead to distinct pressure-drop and heat-transfer responses, even at fixed porosity [59,97].

While permeability characterizes bulk transport, local heat-transfer enhancement depends on solid–fluid interaction mechanisms. Reducing porosity increases ligament density and promotes more frequent boundary-layer interruption, wake interaction, and local mixing. Park et al. [24] reported that increasing relative density from 7.5% to 15% increased average Nusselt number by up to 56.4%, accompanied by intensified turbulent kinetic energy. Similar trends were reported by Qian et al. [68] and Yun et al. [98], who observed enhanced convective coefficients at lower porosity due to increased surface blockage and flow disturbance, albeit with higher pressure-drop penalties.

The resulting trade-off is Reynolds-number-dependent. At lower Reynolds numbers, increased surface exposure and solid conduction pathways can elevate Nusselt number with moderate hydraulic cost. As Re increases, inertial form-drag contributions grow more rapidly, and pressure-drop escalation may outpace heat-transfer gains. Under such conditions, thermal-hydraulic efficiency has been reported to decline despite continued increases in heat-transfer coefficient [44,45]. These trends underscore that porosity must be interpreted within a coupled geometry-flow framework rather than as an isolated predictor of performance.

4.2. Strut Diameter and Geometric Aspect Ratio

The dimensions of individual ligaments significantly influence forced-convection behavior in lattice heat sinks, although their effects are typically observed as part of coupled geometric variations rather than as isolated parameters [20,99]. In most parametric investigations, ligament diameter is adjusted to control relative density and porosity, thereby simultaneously modifying pore size, hydraulic diameter, and internal flow pathways. Con-

sequently, measured thermal-hydraulic trends reflect coupled geometric effects rather than independent variation of ligament diameter.

Consistent with the porosity trends discussed in Section 4.1, increasing strut diameter raises relative density and reduces permeability, whereas thinner ligaments correspond to more open flow passages. Son et al. [74] reported that decreasing porosity through increased ligament diameter in tetrahedral lattice-frame materials produced higher friction factors and elevated Nusselt numbers, indicating intensified solid–fluid interaction and stronger flow disturbance. However, because diameter variation inherently modifies porosity, pore size distribution, and flow tortuosity simultaneously, observed performance changes cannot be attributed solely to strut thickness as an independent variable.

Geometric aspect ratio, defined through characteristic cross-sectional proportions of the struts, introduces additional sensitivity. Ahn et al. [100] varied strut cross-sectional aspect ratio in an FCCZ (FCC with vertical strut) lattice while maintaining nominally constant porosity and topology, and reported measurable changes in flow uniformity, friction factor, and Colburn j factor ($j = \mathrm{Nu}/(\mathrm{RePr}^{1/3})$, where Pr is the Prandtl number) across a range of Re. Fundamental studies of bluff-body wakes further indicate that cross-sectional aspect ratio governs separation mode, vortex shedding characteristics, and wake persistence [101], providing physical insight into how geometric proportion influences internal flow structure within lattice networks. These effects are Re dependent and interact with confinement conditions, suggesting that aspect ratio modifies transport behavior even when global porosity remains fixed.

Beyond hydrodynamics, ligament dimensions define the effective solid conduction network. Conjugate heat-transfer analyses show that variations in strut thickness and connectivity alter effective solid-phase transport while simultaneously reshaping convective heat-transfer behavior [20,23]. Structural parameters governing cross-sectional area and ligament connectivity influence both heat-spreading capability and internal flow distribution. Performance trends therefore cannot be interpreted solely through permeability or surface-interaction metrics, as geometric modifications simultaneously alter both thermal diffusion pathways and fluid-side transport processes. These findings underscore the inherently conjugate nature of heat transfer in lattice heat sinks, where optimal design requires coordinated control of solid conduction and fluid convection.

While strut diameter provides a direct geometric control parameter in discrete-ligament lattices, an analogous role in TPMS structures is played by wall thickness and level-set parameters defining the implicit surface. Variations in TPMS wall thickness simultaneously modify relative density, hydraulic diameter, and conduction pathways, thereby influencing both fluid-side heat transfer and solid-phase heat conduction [59,102]. Similar to strut-based systems, increasing wall thickness enhances surface area and conduction connectivity but also increases flow resistance, reinforcing that geometric effects in both architecture classes arise from coupled modifications of flow and thermal fields rather than independent parameters.

4.3. Unit-Cell Topology and Orientation Relative to Flow

Beyond individual ligament dimensions, unit-cell topology and its orientation relative to the mean flow direction exert a strong influence on forced-convection behavior. Comparative studies under similar porosity conditions indicate that topology significantly alters internal vortex structure, thermal development, and hydraulic resistance. Liang et al. [46] compared staggered pin-fin, Kagome, and BCC arrays at the same porosity of $\varepsilon = 0.88$ and reported endwall Nu increases of 17–24% and 26–41% for the Kagome and BCC arrays compared to pin-fin configurations, attributing enhancement to intensified mixing, horseshoe vortices, and counter-rotating vortex structures. Liang et al. [44] further demonstrated

that, within a single FCC topology at $\varepsilon = 0.92$, variations in ligament orientation were associated with periodic acceleration–deceleration behavior and 25–31% differences in heat-transfer performance. Similarly, Aider et al. [23] reported topology-dependent variations in thermal development and pressure-drop characteristics among periodic lattices at comparable porosity, while Liang et al. [47] linked vortex-scale flow structures directly to convective enhancement across lattice types. Collectively, these studies suggest that topology influences separation behavior, wake interaction, and mixing intensity, thereby modulating both Nu and friction factor even at similar porosity levels.

For TPMS architectures, topology plays an even more intrinsic role, as it directly defines the continuous flow pathways and surface curvature distributions within the structure. Different TPMS families, such as Gyroid, diamond, primitive, and Fischer–Koch S, exhibit distinct flow tortuosity, mixing characteristics, and pressure-drop behavior due to differences in channel connectivity and curvature continuity [97,103]. For instance, Gyroid structures are often associated with relatively low flow resistance and balanced thermo-hydraulic performance, whereas more complex TPMS topologies can enhance mixing but incur higher pressure penalties [59,60].

However, the geometric features that intensify mixing also increase projected frontal area, flow obstruction, and effective tortuosity, amplifying inertial losses. Ferroni et al. [104] showed that decreasing cell size under comparable porosity conditions increases specific surface area while substantially increasing pressure drop (Δp), reflecting the combined growth of viscous and inertial resistance. In lattice heat-sink experiments, Vaglio et al. [27] reported that reducing BCC strut pitch enhanced heat transfer but markedly increased pressure loss, whereas less disruptive staggered configurations exhibited lower Δp alongside reduced thermal performance. Similarly, Shahid et al. [105] compared oblique inline and oblique-staggered Schwarz-TPMS structures and found that staggered layouts promoted stronger transverse mixing and higher Nu, but at the expense of increased hydraulic resistance. These results illustrate the inherent mixing-pressure-loss trade-off associated with topology-driven flow disruption.

Comparative evidence further indicates that topology does not determine performance independently of orientation and boundary conditions. Yahya et al. [106] showed that rotating unit-cell orientation within confined channels significantly altered both Nu and Δp trends, demonstrating that orientation governs the manifestation of topology-driven mixing and blockage effects. Padrão et al. [20] additionally reported that different lattice types experience different effective Reynolds numbers at identical inlet velocities due to variations in hydraulic diameter and internal flow area, complicating direct comparison. This normalization sensitivity is reinforced by Bernardini et al. [107], who showed that Δp correlations depend strongly on hydraulic-diameter definition and flow-direction assumptions, and by Al-Safadi et al. [34], who emphasized that inconsistent Re definitions and boundary-condition reporting contribute substantially to discrepancies across studies. Without consistent specification of unit-cell orientation, confinement conditions, and Re normalization, direct comparison of Nu and Δp trends across lattice topologies may therefore lead to misleading conclusions.

Together, the preceding analyses of porosity, ligament dimensions, and topology indicate that geometric effects operate across multiple interacting length scales. This coupling becomes further complicated under channel confinement conditions, as discussed below.

4.4. Channel Confinement and Lattice–Wall Interaction

The degree of channel confinement and the interaction between lattice structures and bounding walls constitute additional geometric variables that strongly influence forced-convection performance. In confined channels, lattice inserts can reduce bypass flow

and redistribute the working fluid toward the lattice core and heated surfaces, thereby increasing effective surface utilization and strengthening solid–fluid coupling [106,108]. Park et al. [24] further reported that lattice cores tested under confined channel conditions exhibited heat-transfer distributions distinct from those observed for isolated lattice blocks, underscoring the role of confinement in shaping near-wall thermal development.

In TPMS-based configurations, confinement effects can further alter flow distribution due to the bicontinuous nature of the structure, which enables simultaneous transport through multiple interconnected channels. Under confinement, these pathways can promote more uniform flow redistribution and temperature fields, but may also intensify wall-induced shear and pressure gradients depending on blockage ratio and channel geometry [72,97].

Beyond thermal redistribution effects, confinement modifies hydraulic behavior by increasing effective blockage and restricting lateral wake expansion. Although many foundational studies were conducted on canonical bluff bodies, their findings provide mechanistic insight applicable to lattice-induced flow obstruction. Ooi et al. [109] systematically varied blockage ratio (β = 0–0.7) for a confined cylinder at Re = 3900 and showed that increasing confinement accelerates flow through reduced lateral gaps, intensifies wall shear layers, and strengthens adverse pressure gradients, thereby enhancing interaction between wall boundary layers and the wake. Consistently, the review by Mondal and Alam [110] reports monotonic increases in drag coefficient with blockage ratio, reflecting amplification of both viscous and inertial loss mechanisms under restricted lateral expansion. Kalogirou et al. [111] similarly describe how confinement constrains wake development and enhances wall-induced vorticity, altering pressure distributions and vortex organization. Collectively, these studies indicate that increased blockage constrains wake development and intensifies wall-induced shear, leading to elevated hydraulic losses under confinement.

In lattice and cellular heat sinks, confinement effects interact with Re scaling. As Re increases, enhanced cross-stream mixing may coexist with disproportionately increasing pressure-drop penalties due to strengthened form drag and inertial contributions. Comparative investigations of confined lattice and cellular channels report that geometric configurations promoting strong transverse motion also exhibit accelerated pressure-drop growth under increasing blockage [104,105]. These results suggest that thermal-hydraulic performance measured in isolated unit-cell studies or weakly confined test sections may not directly translate to compact heat-sink assemblies integrated within electronic modules.

Meaningful evaluation therefore requires analysis under realistic confinement ratios and boundary conditions representative of power-electronics cooling environments, where lattice–wall interaction strongly influences both heat-transfer distribution and overall pressure-drop behavior.

4.5. Implications for Comparative Assessment

Taken together, the preceding analyses show that forced-convection performance in lattice heat sinks arises from the coupled interaction of porosity, ligament dimensions, unit-cell topology, orientation, and confinement rather than from any single geometric descriptor. Variation in one parameter typically induces concurrent changes in permeability, surface-area density, hydraulic diameter, wake structure, and effective Re scaling, rendering thermal-hydraulic behavior inherently multi-parameter- and regime-dependent.

Consequently, discrepancies in reported heat-transfer and pressure-drop trends across the literature often reflect differences in geometric coupling and confinement conditions rather than contradictions in underlying physical mechanisms. Direct comparison between

studies employing distinct geometric configurations or operating regimes can therefore obscure otherwise consistent thermo-fluid behavior.

These observations highlight the limitations of single-parameter geometric optimization. Meaningful design assessment therefore requires coordinated evaluation of interacting geometric descriptors within defined operating regimes, as further examined through performance metrics in Section 5.

5. Thermal-Hydraulic Performance Metrics and Scaling Considerations

Building on the coupled-geometry perspective established in the previous section, meaningful evaluation of lattice-based heat sinks requires performance metrics that simultaneously capture heat-transfer enhancement and hydraulic cost. Improvements in Nu alone do not indicate superior system-level performance when accompanied by disproportionate increases in pressure drop and pumping power.

Across the literature, inconsistent choices of performance indicators, Re definitions, characteristic length scales, and normalization procedures have contributed to divergent conclusions regarding the relative merit of different lattice geometries. Under one scaling framework, a configuration may appear highly advantageous; under another, its benefit may diminish once hydraulic penalties are accounted for.

This section therefore examines the principal thermal-hydraulic performance metrics employed in lattice heat-sink studies and analyzes how scaling definitions influence comparative assessment and design interpretation.

5.1. Heat Transfer Metrics and Nusselt Number Normalization

The Nusselt number remains the principal metric for quantifying convective heat transfer performance in lattice heat sinks. However, reported Nu values are highly sensitive to the choice of characteristic length, bulk temperature definition, and velocity scale used in the Re normalization.

In conventional duct flows, the channel hydraulic diameter provides a consistent reference length. In lattice heat sinks, multiple geometric length scales coexist, including channel hydraulic diameter, pore size, ligament diameter, and effective scales derived from porosity or surface-area density. Accordingly, normalization strategies vary depending on whether the lattice is modeled as a porous medium, a channel insert, or a periodic unit cell [20,23,51]. This variability complicates direct comparison across studies.

For clarity, the Reynolds number is commonly written as

$$Re = \frac{\rho_f U_{in} D_h}{\mu_f}, \tag{7}$$

where U_{in} is the inlet mean velocity and D_h is the characteristic hydraulic diameter. In lattice and TPMS channels, however, D_h is not unique. Depending on the study, it may be based on the channel cross-section, pore scale, unit-cell size, channel height, strut diameter, or wetted surface area. A frequently used volume-to-area definition is

$$D_h = \frac{4V_c}{A_s}, \tag{8}$$

where V_c is the channel or fluid volume and A_s is the wetted heat-transfer surface area. An equivalent form sometimes used for porous or cellular structures is

$$D_h = \frac{4\varepsilon}{A_{ss}}, \tag{9}$$

where ε is porosity and A_{ss} is the specific surface area. Caket et al. [69] emphasized that studies on lattice metal frames use different characteristic lengths for Reynolds and Nusselt numbers, including channel height, strut diameter, pore diameter, unit-cell length, and hydraulic diameter, which prevents straightforward comparison unless the normalization is clearly stated.

The convective heat-transfer coefficient is commonly obtained from

$$h = \frac{q''}{T_w - T_m}, \tag{10}$$

where q'' is the imposed or measured heat flux, T_w is a representative wall or fluid–solid interface temperature, and T_m is the bulk mean fluid temperature. The Nusselt number is then defined as

$$Nu = \frac{hD_h}{k_f}. \tag{11}$$

Consequently, Nu values reported in different studies should not be compared unless the definitions of D_h, T_w, T_m, velocity scale, and thermal boundary condition are consistent [32,34,69].

Based on these inconsistencies, this review recommends a two-level Reynolds-number reporting strategy. For device-level comparison between lattice heat sinks and conventional fins, microchannels, or cold plates, Reynolds number should preferably be reported using the externally imposed bulk inlet velocity and a channel-level hydraulic diameter,

$$Re_{ch} = \frac{\rho_f U_{in} D_{h,ch}}{\mu_f}, \tag{12}$$

because this definition is most directly linked to the imposed flow rate, pressure drop, and pumping power requirement. For pore-scale or unit-cell-level mechanistic interpretation, a secondary local Reynolds number may also be reported as

$$Re_p = \frac{\rho_f U_p L_p}{\mu_f}, \tag{13}$$

where U_p is a representative pore or interstitial velocity and L_p is a pore diameter, ligament diameter, or unit-cell length. However, Re_p should be treated as a supplementary descriptor rather than the primary comparison basis, because pore-scale definitions vary strongly between strut-based and TPMS architectures.

Accordingly, future studies should report at minimum: (i) the characteristic length used in Re; (ii) whether the velocity scale is inlet, superficial, interstitial, or pore-scale; (iii) porosity ε, wetted surface area A_s, and hydraulic diameter D_h; and (iv) the comparison basis, such as equal flow rate, equal Re, equal pressure drop, or equal pumping power. This two-level reporting strategy preserves a common device-level normalization for cross-study comparison while retaining pore-scale Re as a mechanistic descriptor for explaining local transport behavior [32,34,69].

Furthermore, increases in Nu do not necessarily imply superior heat-sink performance. In confined or low-porosity lattices, geometric reduction of effective flow area can elevate local velocities and apparent Re, increasing convective coefficients while simultaneously producing disproportionate pressure-drop penalties. Liang et al. [44] and Ferroni et al. [104] both documented cases in which geometric constriction enhanced heat transfer coefficients but significantly amplified hydraulic resistance, illustrating that elevated Nu values may reflect flow acceleration rather than intrinsic thermo-fluid improvement.

Additional ambiguity arises from inconsistent use of superficial versus interstitial velocity definitions. Al-Safadi et al. [34] demonstrated that variations in Re formulation and boundary condition reporting contribute substantially to discrepancies in reported thermal-hydraulic performance. Without clearly defined scaling conventions, comparisons based solely on Nu magnitude can obscure physically consistent trends. Nusselt number should therefore be interpreted within a clearly defined geometric and scaling framework rather than as a standalone indicator of performance.

5.2. Pressure-Drop Metrics and Pumping Power Considerations

Pressure drop constitutes a critical constraint in forced-convection lattice heat sinks because it governs the auxiliary energy required to sustain coolant flow. In lattice architectures, hydraulic resistance arises from a combination of viscous wall shear and form drag associated with ligament obstruction, flow separation, wake interaction, and geometric tortuosity. Relative to straight-channel or conventional finned configurations, lattice networks can exhibit increased projected obstruction and repeated acceleration–deceleration regions, which enhance inertial contributions to pressure loss, particularly at moderate to high Reynolds numbers [27,104].

Pressure drop is commonly reported as Δp, $\Delta p/L$ (L is the length), or friction factor (f) as a function of Re. However, interpretation of these quantities requires care. Because the classical Darcy–Weisbach friction factor is defined using inertial scaling, it may decrease with Re even while the dimensional pressure drop increases with flow rate. de Souza Mendes [112] demonstrated that this apparent decrease arises from normalization rather than from reduced mechanical energy dissipation. By reformulating the friction group using viscous-force scaling, the author showed that friction remains constant in laminar flow and increases monotonically with Re in turbulent flow, clarifying the growth of inertial contributions to hydraulic resistance. These analyses indicate that friction-factor trends should be interpreted alongside dimensional pressure-drop data to avoid mischaracterizing inertial amplification.

The hydraulic penalty is commonly quantified using the friction factor. A typical definition is

$$f = \frac{2\Delta p D_h}{\rho_f U_{in}^2 L}, \tag{14}$$

where Δp is the pressure drop over the lattice length L. Some studies instead define the friction factor using wetted area, pore-scale quantities, permeability, or channel height. Therefore, similar to Nu, the friction factor must be interpreted together with its definition and characteristic length [34,69].

From a system-level perspective, pumping power,

$$P_{\text{pump}} = \Delta p \dot{V}, \tag{15}$$

where $\dot{V}$ is the volumetric flow rate, provides a more direct measure of hydraulic cost than pressure drop alone. Because $\dot{V}$ increases with velocity, pumping power scales with both pressure drop and flow rate and therefore grows more rapidly with velocity in inertia-dominated regimes.

These considerations indicate that pressure-drop data should be evaluated together with flow-rate scaling and pumping power implications. Reporting Δp or friction factor without explicit reference to operating regime and energy consumption can lead to incomplete assessment of practical suitability in compact power-electronics cooling applications.

Thermal-Hydraulic Efficiency and Performance Factor

To reconcile heat transfer enhancement with hydraulic penalty, studies on lattice heat sinks commonly employ thermal-hydraulic performance indicators that combine Nu and pressure-drop information into a single comparative index. A widely adopted formulation is the performance evaluation criterion (PEC), expressed as

$$\eta = \left(\frac{Nu}{Nu_0}\right)\left(\frac{f_0}{f}\right)^{1/3} \tag{16}$$

where Nu_0 and f_0 denote the Nusselt number and friction factor of a reference geometry evaluated at identical Re conditions. This formulation is commonly interpreted as representing comparison at equal pumping power and enables normalized assessment relative to smooth channels, empty ducts, or conventional fin arrays [22,29].

The exponent $1/3$ arises from equal-pumping power scaling. For geometrically comparable forced-convection channels, pressure drop scales approximately with fU^2, while volumetric flow rate scales with U. Therefore, $P_{\text{pump}} = \Delta p\dot{V}$ scales approximately with fU^3. If an enhanced geometry has a higher friction factor than the reference geometry, the velocity allowed at equal pumping power is reduced by a factor proportional to $(f_0/f)^{1/3}$. The term $(f_0/f)^{1/3}$ therefore penalizes heat-transfer enhancement by the hydraulic cost associated with increased friction [32,38,69,113].

In addition to η or PEC-type metrics, several studies use alternative performance indices such as $Nu/f^{1/3}$, j/f, and $j/f^{1/3}$. Here, j is the Colburn heat-transfer factor, defined as

$$j = StPr^{2/3}, \tag{17}$$

where St is the Stanton number and Pr is the Prandtl number. Since

$$St = \frac{Nu}{RePr}, \tag{18}$$

the Colburn factor can also be written as

$$j = \frac{Nu}{RePr^{1/3}}. \tag{19}$$

The j-factor combines heat-transfer performance with the effects of Reynolds and Prandtl numbers, allowing convective performance to be compared more compactly across different flow conditions [34,69].

Heat-transfer rate per unit pumping power, Q/P_{pump}, is another useful cost–benefit metric because it directly compares useful thermal transport with hydraulic power input:

$$\frac{Q}{P_{\text{pump}}} = \frac{\dot{m}c_{p,f}(T_{out} - T_{in})}{\Delta p\dot{V}}, \tag{20}$$

where $Q = \dot{m}c_{p,f}(T_{out} - T_{in})$ is the heat-transfer rate, $\dot{m}$ is the mass flow rate, and T_{out} and T_{in} are the outlet and inlet fluid temperatures, respectively. A higher Q/P_{pump} indicates that more heat is transferred for a given hydraulic energy input, which is particularly relevant for practical heat-sink and heat-exchanger design [34].

While convenient, the interpretive value of PEC depends strongly on the selected baseline geometry, Re definition, and confinement condition. Dixit et al. [22] showed that configurations ranking favorably based on heat-transfer coefficient alone may exhibit reduced PEC values once friction penalties are incorporated. Similarly, Batikh et al. [28] reported that certain lattice heat sinks outperform straight-fin baselines only within specific Re ranges, with relative performance diminishing as inertial losses intensify.

Across structured channels and lattice-based systems, thermal-hydraulic efficiency often decreases with increasing Re in inertia-dominated regimes. Although Nu generally increases with flow rate, friction factor and dimensional pressure-drop growth may scale more steeply due to enhanced form drag and wake persistence [44,45]. Consequently, the friction-related term in the PEC formulation can increase more rapidly than the heat transfer ratio, leading to a reduction in η at a higher Re for geometries characterized by strong flow disruption.

A performance factor exceeding unity therefore indicates improvement relative to the chosen baseline at a specified operating condition, but does not imply universal superiority across Re ranges or confinement levels.

5.3. Reynolds-Number Dependence and Scaling Behavior

The forced-convection performance of lattice heat sinks exhibits pronounced Re dependence arising from the evolving balance between viscous transport, wake-induced mixing, and inertial form drag. At low to moderate Re, convective enhancement is typically associated with boundary-layer disruption and localized acceleration–deceleration within the ligament network. Under such conditions, increasing Re generally produces measurable gains in Nu, while hydraulic penalties increase more gradually [24,44].

As Re increases further, inertial effects become increasingly dominant. Intensified separation, persistent wake structures, and repeated flow redirection within the lattice amplify form-drag contributions, leading to a more rapid rise in pressure drop relative to heat transfer enhancement. Experimental and numerical investigations of lattice and cellular heat sinks report that although Nu continues to increase with Re, the associated growth in dimensional pressure drop often accelerates more strongly [27,45,114]. This disparity in scaling frequently results in reduced thermal-hydraulic performance indicators at higher Reynolds numbers, as discussed above.

Such Re sensitivity implies that lattice geometries cannot be evaluated independently of their intended operating regime. Configurations designed to promote strong cross-stream mixing and wake interaction may exhibit favorable performance within moderate Re ranges but incur substantially higher hydraulic penalties as inertial contributions intensify. Conversely, more flow-aligned or less obstructive architectures may provide comparatively modest enhancement at low Reynolds numbers while maintaining more stable thermal-hydraulic efficiency as Re increases.

Accordingly, scaling trends reported across the literature should be interpreted alongside geometric confinement, porosity level, and normalization definitions. Differences in Re range, velocity basis (superficial versus interstitial), and hydraulic-diameter selection can shift apparent performance rankings. Apparent contradictions in reported trends may therefore reflect differences in operating regime and scaling methodology rather than fundamental disparities in lattice topology.

5.4. Quantitative Benchmarking Envelope Across Surveyed Studies

The preceding discussion shows that a single universal benchmark for lattice and TPMS heat sinks would be misleading because the surveyed studies use different Reynolds-number definitions, characteristic lengths, hydraulic diameters, baseline geometries, coolants, thermal boundary conditions, and comparison bases. Nevertheless, a need remains for order-of-magnitude guidance on the expected thermal and hydraulic performance of lattice and TPMS heat sinks. Therefore, instead of forcing all data into one universal correlation, the present review introduces a benchmarking-envelope approach. In this approach, reported thermal gains and hydraulic penalties are grouped according to the

original comparison basis used in each study, such as equal Reynolds number, equal pumping power, similar pressure drop, or comparison against a specific conventional baseline.

To improve transparency, Table 3 summarizes representative quantitative ranges from the surveyed literature. The reported values are not re-normalized across studies; rather, they are retained in the form reported by the original authors or review sources. This avoids artificial precision while still providing readers with practical order-of-magnitude expectations for thermal enhancement and hydraulic cost.

The benchmark ranges in Table 3 indicate that lattice and TPMS architectures can provide modest to very large thermal enhancement depending on topology and comparison basis. Relative to plate-fin or zigzag-type compact baselines, reported improvements commonly fall within the range of tens of percent and, in selected TPMS cases, exceed 100%. However, the corresponding hydraulic penalty can also be substantial. For example, some TPMS-to-zigzag comparisons report friction-factor increases of approximately 50–100%, while fin-assisted TPMS designs report pressure-drop increases over the examined flow-rate and fin-height ranges. Therefore, the relevant engineering question is not whether the lattice increases (Nu), but whether the increase in (Nu), (h), or (Q) outweighs the increase in (f), (Δp), and pumping power.

A useful way to interpret the surveyed data is through the qualitative benchmarking map shown in Figure 5. The vertical axis represents thermal enhancement, such as (Nu/Nu_0), (h/h_0), or (Q/Q_0), while the horizontal axis represents hydraulic penalty, such as (f/f_0), ($\Delta p/\Delta p_0$), or ($P_{\text{pump}}/P_{\text{pump},0}$). Because the reviewed studies do not use a single common baseline, the map is intentionally presented as a design-envelope framework rather than as a precise scatter plot.

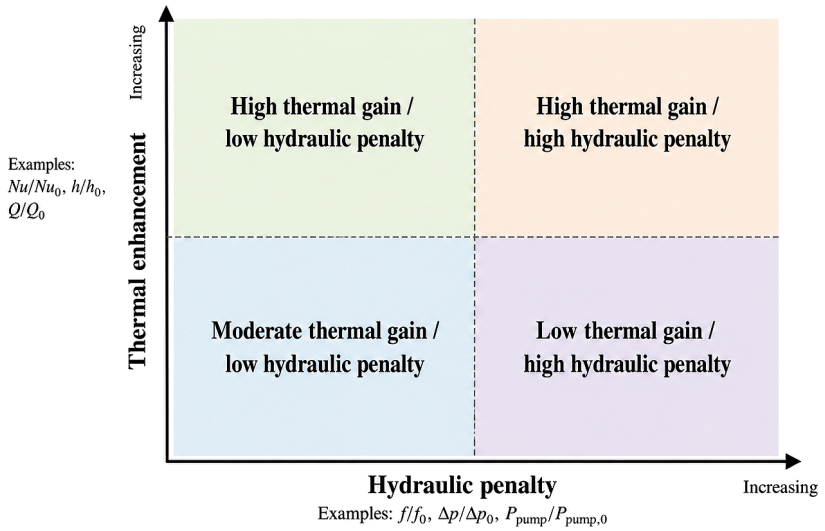


Figure 5. Conceptual benchmarking map for lattice and TPMS heat-transfer structures.

The benchmarking envelope clarifies several practical trends. First, TPMS and lattice designs are most compelling when thermal enhancement is reported at equal pumping power or similar pressure drop, because these comparisons already include the hydraulic cost. Second, very high (Nu) or heat-transfer-coefficient enhancement alone can be misleading if achieved through severe flow blockage or high tortuosity. Third, geometry modifications can sometimes improve both heat transfer and hydraulic performance, as reported for controlled Gyroid deformation, but this behavior is not universal. Fourth, conventional compact-channel heat sinks may still outperform TPMS structures in low-Reynolds-number or pumping power-limited regimes. These observations support the

use of benchmarking envelopes and performance maps, rather than isolated enhancement ratios, when assessing practical lattice heat-sink viability.

Table 3. Representative quantitative benchmarking envelope for lattice and TPMS heat-transfer structures. Values are retained using the comparison basis of the original studies; therefore, the ranges should be interpreted as order-of-magnitude guidance rather than a universal correlation.

Study/Source	Configuration and Baseline	Thermal Enhancement	Hydraulic Penalty/Interpretation
Wang et al. [32]; based on Tang et al. [52]	TPMS heat sinks compared with conventional plate-fin heat sinks	Nusselt-number enhancement of approximately 5.8–196%, depending on TPMS topology and operating condition	Enhancement accompanied by increased pressure drop; PEC-type evaluation is required.
Yeranee and Rao [38]	Gyroid and Diamond TPMS heat exchangers compared with zigzag-type compact channels	Nusselt-number increase of approximately 30–65%; thermal-performance improvement of approximately 17–100%	Friction factor approximately 50–100% higher in the cited comparisons.
Dharmalingam et al. [37]	TPMS heat exchangers compared with printed-circuit heat-exchanger designs	Heat-transfer coefficients approximately 15–120% higher	Reported at a given pumping power; hydraulic cost is partly embedded in the comparison.
Dharmalingam et al. [37]	Fischer–Koch TPMS designs compared with Schwarz-D TPMS design	Heat-transfer increase of approximately 23–356%	Reported at similar pressure drop relative to Schwarz-D in the cited computational comparison.
Caket et al. [69]	Single-layer lattice metal-frame channels compared using channel height as characteristic length	X-type OA arrangement reported the highest Nusselt number among compared LMFs	X-type OA also produced the highest friction factor; X-type OB showed the highest efficiency index.
Al-Safadi et al. [34]	Gyroid TPMS heat-sink data compared with compact-channel heat-sink data using heat transfer per unit pumping power	TPMS was not always superior when evaluated using Q/P_{pump}	Conventional compact-channel heat sinks performed better at low Reynolds numbers below approximately $Re = 800$ in the cited comparison.
Tang et al. [115]	Controlled deformation of Gyroid-type TPMS lattice structure	Increasing deformation parameter increased average heat-transfer coefficient by 19.9–28.9% and Nusselt number by 0.3–4.5%	Average friction factor decreased by 13.0–20.3%; geometry control can improve heat transfer without increasing flow resistance.
Tang et al. [116]	TFS-Gyroid heat sink with added fin structures	Average surface convective heat-transfer coefficient increased by 27.4–34.6%	Pressure drop increased from 42.5 to 632.8 Pa as fin height increased from 0 to 1.6 mm; PEC may decrease due to pressure-drop growth.

5.5. Implications for Comparative Assessment and Design Practice

The preceding analysis indicates that no single metric, whether Nu, friction factor, or pressure drop, can independently characterize the performance of lattice-based heat sinks. Because geometric parameters simultaneously influence surface interaction, flow structure, hydraulic resistance, and effective Re scaling, meaningful comparison requires integrated evaluation within a consistent normalization framework. Comparative assessment should therefore explicitly specify: (i) the characteristic length and velocity definitions used in Nusselt-number calculation; (ii) the pressure-drop metric and scaling adopted (e.g., Δp, $\Delta p/L$, or friction factor), together with the corresponding reference length and hydraulic-diameter definition; and (iii) the baseline configuration employed for performance-factor evaluation. Without such transparency, reported enhancement may primarily reflect differences in normalization methodology rather than intrinsic geometric advantage.

From a design perspective, heat transfer enhancement alone is an insufficient decision criterion. In energy-conversion and power-electronics cooling systems, where auxiliary pumping power directly influences efficiency and sustainability, the relevant objective is not maximizing Nu, but achieving improved heat-transfer effectiveness at an acceptable hydraulic cost. Thermal-hydraulic performance metrics and regime-specific performance maps, such as the conceptual framework illustrated in Figure 4, therefore provide a more robust basis for identifying operating windows in which lattice geometries deliver tangible system-level benefit.

Accordingly, rational design practice should move beyond single-parameter optimization toward regime-aware, multi-parameter evaluation strategies that explicitly account for Re dependence, confinement effects, and geometric coupling. Only within such a balanced framework can lattice heat sinks be fairly assessed against conventional cooling technologies and deployed where their structural complexity translates into genuine thermal-hydraulic advantage.

6. Manufacturing, Materials, and Practical Constraints

Although lattice-based heat sinks often demonstrate favorable thermo-fluid performance under controlled forced-convection conditions, practical deployment in power-electronics cooling is governed by manufacturing feasibility, material behavior, scalability, and system-level integration. Geometries optimized under idealized numerical or laboratory environments may exhibit dimensional deviations, surface variability, or altered flow distribution once realized as physical components. Accordingly, the viability of lattice heat sinks depends on coordinated alignment between thermal-hydraulic performance, manufacturability, material properties, and integration within compact energy systems.

6.1. Additive Manufacturing Constraints Relevant to Heat Transfer

Additive manufacturing (AM) enables fabrication of lattice geometries with high surface-area density and complex three-dimensional connectivity that are difficult to achieve using conventional processes [117]. However, process-specific constraints directly influence thermo-fluid performance. Minimum feature size, powder-removal requirements, and layer-wise fabrication limit achievable ligament diameters and pore dimensions, thereby constraining attainable combinations of porosity and surface-area density [118]. Designs approaching these limits may exhibit dimensional deviation and surface irregularities, characteristic of powder-bed fusion, including partially fused particles, stair-stepping effects, and melt-pool-induced roughness [119–121].

As-built surface roughness further modifies forced-convection behavior. Compared with smooth CAD geometry, experimentally measured roughness in AM lattices has been shown to alter heat-transfer and pressure-drop predictions by tens of percent under turbu-

lent conditions [122,123]. Experimental comparisons between additively manufactured and conventionally fabricated heat exchangers likewise confirm that manufacturing-induced surface and microstructural features influence both heat-transfer coefficients and hydraulic resistance [124,125]. Because roughness magnitude and morphology depend on fabrication route and processing parameters, performance trends are not universally transferable across AM methods.

As-built surface condition should therefore be treated as an intrinsic geometric characteristic rather than a secondary correction to idealized CAD representations.

6.2. Manufacturing-Induced Deviations and Their Thermo-Hydraulic Consequences

Although additive manufacturing enables fabrication of lattice and TPMS heat sinks with complex internal geometries, the as-built structure often differs from the nominal CAD model. This difference is important because thermal-hydraulic performance depends not only on the designed topology, porosity, and wall thickness, but also on the manufactured surface morphology, dimensional accuracy, internal defects, and post-processing condition. Therefore, manufacturing constraints should be interpreted as performance-controlling factors rather than only fabrication limitations.

The relationship between manufacturing parameters and thermal-hydraulic behavior can be understood through the following causal pathway:

$$\begin{aligned} &\text{AM parameters} \rightarrow \text{as-built deviations} \\ &\rightarrow D_h,\ A_s,\ \varepsilon,\ k_{\text{eff}},\ \text{roughness} \\ &\rightarrow Nu,\ f,\ \Delta P,\ PP,\ \eta \end{aligned} \tag{21}$$

At the process level, laser power, scanning speed, layer thickness, hatch spacing, build orientation, and post-processing directly affect relative density, wall thickness, porosity distribution, surface morphology, dimensional accuracy, and structural integrity [41]. For TPMS structures, this sensitivity is amplified because the geometry contains thin walls, continuously curved surfaces, overhang regions, and interconnected internal channels. In powder-bed-fusion processes, partially melted powder, sticking powder, staircase effects, overhang roughness, and melt-pool instability can produce deviations in wall thickness, pore size, surface roughness, and porosity [32,38,41].

These deviations have direct thermal-hydraulic consequences. Surface roughness and attached powder increase the effective wetted surface area and can disturb the near-wall boundary layer, which may enhance local convective heat transfer. However, the same roughness also increases wall shear, flow blockage, pressure drop, and pumping power demand. Yeranee and Rao [38] reported that surface roughness and sticking powder in PBF-fabricated TPMS cooling channels increase pressure loss, while micro-voids and micro-cracks can reduce the thermal conductivity of the heat sink. Similarly, Wang et al. [32] noted that sticking powder, overhang effects, and staircase effects alter the real fluid–solid interface, disturb the flow field, and affect both flow resistance and thermal performance.

Quantitative evidence also shows that these deviations are not negligible. Wang et al. [32] reported that SLM-fabricated Gyroid, Diamond, and Primitive heat sinks can show measured porosity deviations of up to 5% from the design value. The same review reported porosity deviations of 7–12% in other AM-fabricated TPMS structures and relative-density deviations of 1.54–3.94%. They also reported that CT-based comparison of as-built and CAD geometries showed average deviations of approximately 42.27 μm for sheet-based TPMS structures and 13.31 μm for network structures. These geometric deviations modify the solid volume fraction, effective heat-transfer area, hydraulic diameter, and conductive heat-transfer pathway.

The effect on pressure drop can be particularly strong. Wang et al. [32] reported that pressure-drop predictions based on ideal smooth models can deviate from measurements by up to 69.82%. Al-Safadi et al. [34] similarly highlighted that AM-induced roughness, wall-thickness deviation, and local geometric imperfections contribute to discrepancies between CFD predictions and experiments. In the case discussed by Al-Safadi et al. [34], the pressure-drop deviation reached 44.94% at (Re = 150) and increased to 69.82% near (Re = 1350). This occurs because increased roughness and reduced hydraulic diameter become more influential as the viscous boundary layer becomes thinner with increasing Reynolds number.

Surface roughness may therefore be beneficial or detrimental depending on the selected performance metric. Caket et al. [69] reported that DMLS-manufactured aluminum alloy heat sinks with average surface roughness in the range of 1–25 μm under turbulent conditions achieved approximately 50% higher thermal performance compared with standard manufacturing techniques. However, this type of improvement should not be generalized without considering the associated pressure drop and pumping power. For lattice heat sinks, a rougher surface may increase (Nu), but the net performance improves only if the increase in heat transfer outweighs the increase in (f), (ΔP), and (PP).

Post-processing can reduce the hydraulic penalty while preserving much of the heat-transfer capability. Rashid et al. [39] summarized a study on abrasive jet polishing of an SLM-fabricated gyroid heat exchanger, where polishing reduced the density of protruding internal microstructures. The reported roughness-induced surface-area increase decreased from 106–123% before polishing to 20–45% after polishing, while the pressure drop decreased by approximately 40% and the heat-transfer capacity remained nearly unchanged. Over Re = 300–3000, the polished prototype showed an average overall performance improvement of 12.94–26.09% compared with a counterbalance strip-fin heat exchanger [39]. This evidence shows that surface finishing can shift the thermal-hydraulic balance by reducing flow resistance without necessarily sacrificing heat-transfer capacity.

Despite these reported data, the literature does not yet provide a universal quantitative correlation directly linking AM process parameters to (Nu), (f), or (η) across all lattice and TPMS heat sinks. Such a correlation is difficult because the outcome depends on topology, material, unit-cell size, wall thickness, build orientation, post-processing, flow regime, and the definitions of (D_h), (Nu), and (f). Therefore, the most reliable current approach is to report both nominal design parameters and measured as-built quantities. Future studies should report measured porosity, wall-thickness deviation, pore-size deviation, surface roughness, CT-reconstructed surface area, hydraulic diameter, pressure drop, pumping power, heat-transfer coefficient, and Nusselt number. This reporting practice is necessary to establish physically meaningful relations between manufacturing quality and thermal-hydraulic performance.

6.3. Material Thermal Conductivity and Solid–Fluid Coupling

Material selection influences lattice performance through solid-phase conduction and solid–fluid thermal coupling. Studies on additively manufactured cellular metals consistently report that effective thermal conductivity decreases with increasing porosity due to reduced cross-sectional area and increased conduction-path tortuosity [23,95,126,127]. Effective conductivity scales strongly with relative density in open-cell lattices [95], and topology and strut thickness alter solid conduction pathways under conjugate heat-transfer conditions [23]. These findings confirm that ligament connectivity and cross-sectional area govern internal heat-spreading capability.

Higher intrinsic material conductivity reduces internal temperature gradients [20]. However, in forced-convection systems, the relative contribution of solid conduction and

fluid convection depends on operating regime. At moderate to high Reynolds numbers, fluid-side resistance may become comparable to or dominant over solid conduction resistance, such that geometric parameters influencing mixing and boundary-layer disruption can outweigh incremental gains in material conductivity [44,45].

Material benefits are therefore inseparable from geometry. Increasing porosity or reducing ligament cross-section narrows conduction pathways despite high intrinsic conductivity [94,95]. Material and geometry must thus be treated as coupled design variables.

At the assembly level, interface resistance (e.g., TIM/contact resistance) between the lattice base and the heat source adds a series resistance to the total thermal pathway and can reduce or even offset gains from high-conductivity cores if not controlled or characterized [128]. Realistic assessment of material effects therefore requires integrated evaluation of solid conduction, convection, and interfacial resistance within the complete thermal pathway [92].

6.4. Scalability, Repeatability, and Cost Considerations

Despite laboratory-scale advantages, scalability remains constrained by manufacturing throughput, cost, and quality control. AM build time increases with part volume and feature resolution, and metal powder-bed systems typically incur higher unit costs than mass-produced extruded or stamped heat sinks [117,129,130]. These factors may limit economic feasibility in cost-sensitive energy applications.

Repeatability presents an additional challenge. Documented AM variations in strut thickness, surface roughness, internal porosity, and geometric distortion [118,124] directly affect relative density and pore geometry. Even small dimensional deviations alter permeability and effective thermal conductivity relationships [94,95], influencing both pressure drop and heat-transfer behavior. Such variability complicates reliability assessment and correlation development for applications with narrow thermal margins.

From a sustainability perspective, lifecycle assessments indicate that metal AM processes often exhibit higher production-phase energy intensity than conventional routes [131,132]. The net environmental benefit of lattice heat sinks therefore depends on balancing operational efficiency gains against manufacturing energy demand, material utilization, durability, and service lifetime.

Furthermore, heat-transfer enhancement must be evaluated alongside pumping power implications (Section 5). Geometries that increase local Nusselt number but require higher flow rates or tighter manufacturing tolerances may not yield favorable techno-economic outcomes over the full system lifecycle.

Rigorous comparison should therefore integrate scalability, repeatability, lifecycle energy demand, and cost-per-performance metrics in addition to component-level enhancement.

6.5. Integration and System-Level Constraints

Integration into practical cooling systems introduces constraints absent in isolated channel studies. Packaging limits, allowable system pressure drop, and fan or pump operating characteristics bound achievable mass flow rate and therefore thermal enhancement. In air-cooled modules, available fan pressure head directly constrains mass flow rate [133], defining the admissible operating window.

Application-oriented investigations emphasize that performance must be evaluated under realistic flow budgets and enclosure constraints rather than laboratory-optimal conditions [28]. Controlled inlet conditioning and idealized geometries [24] may not represent installed systems, where confinement and pumping limits modify flow distribution.

Flow maldistribution in compact modules is well documented. Non-uniform inlet conditions and plenum geometry distort local mass flux and alter pressure-drop and

thermal behavior relative to uniform assumptions [134–136]. Because lattice performance is highly sensitive to Reynolds-number scaling and confinement, as discussed in the previous sections, such deviations can shift the system away from the optimized regime.

Mechanical reliability under sustained thermal loading is similarly critical. AM-induced anisotropy, residual stress, and microstructural heterogeneity influence mechanical response [137,138]. Residual-stress simulations report stress concentration at nodes and junctions [139], and fatigue studies demonstrate architecture-dependent durability governed by junction-level stress intensification [140,141]. Thermal cycling may therefore affect long-term structural stability.

Surface roughness and reduced pore dimensions may also increase fouling susceptibility in air-cooled systems, modifying permeability and hydraulic resistance over time [51], although systematic quantification remains limited. Lattice heat sinks must therefore be evaluated as integrated system components whose performance depends on enclosure geometry, interface quality, operating duty cycle, and environmental exposure. Reliable assessment requires representative system-level testing rather than extrapolation from isolated unit-cell studies.

6.6. Implications for Practical Deployment

Practical viability depends on coherent alignment between geometry, material behavior, manufacturability, and system-level constraints. Substantial Nusselt-number enhancement observed under controlled conditions may not translate into net system-level benefit once manufacturing tolerances, surface condition, pumping power limits, and integration constraints are incorporated. Progress therefore requires process-aware geometric design, transparent and normalization-consistent performance characterization, and system-level validation under realistic confinement and duty-cycle conditions. Embedding thermal-hydraulic optimization within a manufacturable, scalable, and application-aware framework is essential for transitioning lattice heat sinks from exploratory demonstrations to deployable thermal-management solutions for high-power energy systems.

7. Limitations, Contradictions, and Research Gaps

Despite substantial experimental and numerical progress, several limitations continue to hinder reliable cross-study comparison and practical deployment of lattice-based heat sinks in power-electronics cooling. Many apparent contradictions arise not from disagreement in the underlying physical mechanisms alone, but from the combined effects of geometric definition, Reynolds-number normalization, boundary-condition specification, manufacturing variability, experimental uncertainty, operating regime, and system-integration context. This section consolidates the principal sources of discrepancy and identifies priority research gaps.

7.1. Discrepancies Between Experimental and Numerical Studies

A persistent challenge in lattice and additively manufactured (AM) heat-sink research is mismatch between numerical simulation predictions and experimental measurements under nominally similar conditions. Manufacturing-induced deviations, such as surface roughness, strut-thickness variation, and geometric imperfection, modify near-wall flow and effective hydraulic diameter, influencing both pressure loss and heat transfer [34].

Simulations commonly employ ideal smooth CAD geometry, whereas experiments reflect as-manufactured surface morphology and dimensional variation. Kaur and Singh [122] reported that neglecting roughness and manufacturing effects can produce heat-transfer prediction deviations exceeding 20%. Incorporation of roughness-informed representations

improved agreement, although residual discrepancies (≈10–30%) remained depending on modeling assumptions.

Experimental uncertainties further contribute to variation. Reported uncertainty budgets associated with flow-rate measurement, pressure instrumentation, and temperature calibration propagate into Nusselt number and friction-factor evaluation [28,44]. Manufacturing tolerances are not always fully captured in derived heat-transfer coefficients [44]. These findings indicate that numerical-experiment mismatch often reflects geometric fidelity and boundary-condition realism rather than deficiencies in governing equations. Rigorous paired validation using documented as-manufactured geometry and transparent uncertainty reporting is therefore essential.

Accordingly, normalization inconsistency should be interpreted as only one source of cross-study discrepancy. Manufacturing repeatability, surface morphology, dimensional tolerance, sensor calibration, heat-loss correction, inlet-flow conditioning, and boundary-condition implementation can also shift the measured or predicted Nu, f, and Δp. Therefore, discrepancies between studies should be evaluated using both normalization consistency and experimental fidelity, rather than being attributed to a single cause.

7.2. Inconsistent Geometric Definitions and Scaling Frameworks

A major source of contradiction stems from inconsistent geometric and normalization conventions. Studies employ different characteristic lengths for Reynolds and Nusselt numbers, including channel hydraulic diameter, pore diameter, ligament diameter, and porosity-derived effective scales [20,23,51]. Some treat lattices as porous media with superficial velocity scaling; others use interstitial or channel-based definitions.

Al-Safadi et al. [34] showed that Reynolds-number formulation and boundary-condition specification materially affect reported heat-transfer and pressure-drop trends. Bernardini et al. [107] similarly demonstrated that hydraulic-diameter definition and assumed flow direction influence pressure-loss correlations and comparative ranking.

Such differences do not imply disagreement in physics, but without transparent reporting of characteristic length, velocity basis, confinement ratio, and reference geometry, normalization artifacts can obscure intrinsic geometric effects. The absence of consistent scaling conventions remains a barrier to meta-analysis and transferable design guidance.

7.3. Limited Coverage of Application-Relevant Operating Regimes

Many lattice heat-sink studies examine Reynolds-number ranges selected for laboratory feasibility rather than alignment with realistic fan- or pump-constrained conditions [24,44]. Although mechanistically informative, such ranges may not correspond to installed electronic modules.

In practical air-cooled systems, achievable mass flow rate is limited by fan pressure-flow characteristics and allowable system pressure drop [133]. Application-oriented studies emphasize evaluation within constrained flow budgets [28,142]. Moreover, as discussed in Section 5, thermal-hydraulic efficiency often declines at elevated Reynolds numbers when inertial losses grow more rapidly than heat-transfer enhancement [44,45].

Without systematic exploration of fan- or pump-constrained operating envelopes, the Reynolds-number regimes in which lattice heat sinks provide net system-level benefit remain insufficiently defined.

7.4. Insufficient System-Level and Long-Term Evaluation

Most investigations assess lattice heat sinks under steady-state, component-level conditions with uniform inlet flow and controlled heat flux [24,44]. Practical assemblies involve non-uniform heat flux, plenum effects, and interaction with upstream and downstream

components [134,135], which can significantly alter local Reynolds-number distribution and pressure-drop behavior.

Thermal contact resistance at the lattice–base interface is frequently underreported. Experimental studies show that interfacial resistance can constitute a significant fraction of total thermal resistance in compact modules [114], potentially offsetting core-level gains.

Long-term reliability is also insufficiently characterized. Additively manufactured lattices exhibit anisotropy, residual stress, and defect sensitivity [137,138], and fatigue studies report junction-level stress concentration effects [140,141]. However, systematic coupling of thermo-fluid performance with mechanical degradation under service conditions remains limited.

Lifecycle considerations, including manufacturing-phase energy intensity, are similarly rarely integrated into performance evaluation [131]. The lack of system-level validation, durability assessment, and lifecycle integration represents a critical gap between laboratory studies and deployment in long-lifetime energy systems.

7.5. Limited Design-Oriented Guidance and Benchmarks

Although numerous lattice geometries have been investigated, relatively few studies translate thermo-fluid findings into transferable design frameworks. Performance is commonly reported relative to a single baseline under narrowly defined conditions [22,44], limiting generalization.

Comparative ranking is often normalization-dependent. Variations in Reynolds-number definition, hydraulic-diameter scaling, and pumping power treatment can materially alter apparent superiority [34,112]. Additionally, many parametric studies emphasize peak Nusselt enhancement without integrating pumping power limits, manufacturability constraints, or enclosure-level considerations [27,45].

The absence of standardized benchmarks, shared reference geometries, and regime-aware performance maps restricts synthesis and actionable engineering guidance.

7.6. Summary of Research Gaps

The preceding analysis indicates that the principal limitations in lattice heat-sink research arise less from insufficient geometric innovation than from fragmentation in scaling methodology, validation practice, and system-level evaluation.

Apparent contradictions frequently originate from inconsistent normalization conventions, limited regime coverage, and inadequate integration of manufacturing, confinement, and durability considerations. As a result, the conditions under which lattice architectures provide reproducible, system-level benefit remain insufficiently defined.

Addressing these gaps requires coordinated advances in normalization consistency, integrated experimental–numerical validation, regime-aware operating-envelope mapping, system-level integration studies, and long-term durability assessment. These priorities define the transition from exploratory geometric enhancement toward deployment-oriented thermal-management research.

8. Future Research Directions and Design Guidelines

The preceding sections demonstrate that lattice-based heat sinks possess significant thermo-fluid potential; however, practical deployment requires a shift from geometry-centered enhancement studies toward normalization-consistent, manufacturable, and system-integrated design frameworks. Future progress depends on establishing reproducible scaling conventions, embedding optimization within realistic operating constraints, and integrating geometric innovation with material behavior, manufacturability, and lifecy-

cle considerations. This section outlines structured research directions aimed at enabling application-relevant, deployment-ready lattice heat-sink design.

8.1. Unified Geometric Descriptors and Scaling Frameworks

Reliable comparison across lattice architectures requires standardized geometric descriptors and normalization conventions. Porosity or relative density alone cannot capture the coupled effects of surface-area density, pore scale, connectivity, and conduction pathways. More informative descriptors should integrate characteristic pore size, specific surface area, hydraulic diameter, and connectivity metrics to link structure with both fluid transport and solid conduction.

Equally critical is consistent scaling of Reynolds number, Nusselt number, and pressure drop. Transparent specification of characteristic length, velocity basis, and temperature reference would reduce ambiguity and enable cross-study synthesis. Adoption of shared geometric and scaling conventions is a prerequisite for transferable performance maps and generalizable design rules.

8.2. Optimization Under Realistic Operating Constraints

Future optimization studies should incorporate pumping power limits, fan/pump performance curves, acoustic constraints, and allowable auxiliary energy consumption. Designs optimized solely for peak heat-transfer enhancement may yield limited system-level benefit once hydraulic penalties are considered. Moderate Reynolds-number regimes often provide the most favorable balance between convective enhancement and pressure-drop cost. Regime-aware optimization targeting realistic operating envelopes, rather than extreme flow conditions, is therefore essential for application-relevant design.

8.3. Coupled Geometry–Material–Manufacturing Design

Practical deployment requires coordinated optimization of geometry, material properties, and manufacturing constraints. Additive manufacturing should be treated not as an enabler of arbitrary geometry, but as a process imposing limits on feature size, surface condition, tolerance, and repeatability. Material selection must be evaluated jointly with ligament thickness, relative density, and operating regime. In convection-dominated systems, incremental increases in intrinsic conductivity may offer diminishing returns unless supported by appropriate geometric design. Integrated optimization incorporating manufacturability and performance variability is more likely to yield deployable solutions than geometry-only enhancement studies.

8.4. System-Level Validation and Durability Assessment

Translation to practice requires a prescriptive validation protocol rather than isolated heat-transfer testing. For lattice heat sinks intended for power-electronics cooling, validation should be performed in a representative module or cold-plate assembly that includes the heat source, baseplate, thermal interface material (TIM), manifold or plenum, enclosure confinement, and the available fan or pump operating range. This is important because the thermal path in power modules includes several resistances, including junction-to-case, case-to-heat-sink, and heat-sink-to-ambient resistances, while cooling performance also depends on coolant flow rate, input power density, ambient temperature, and allowable pressure drop [92].

A minimum system-level validation protocol should therefore include: (i) a baseline comparison against a conventional fin, pin-fin, microchannel, or commercial cold-plate design under the same heat load and flow budget; (ii) steady-state tests under uniform and non-uniform heat-flux maps; (iii) transient power-cycling tests representative of pulsed or duty-cycle operation; (iv) operation along a realistic fan or pump curve rather than only at

prescribed ideal flow rates; and (v) post-test inspection of the lattice for blockage, leakage, deformation, fouling, or structural damage. The reporting metrics should include maximum device or junction temperature T_{max}, surface temperature non-uniformity $\Delta T_{surface}$, thermal resistance R_{th}, heat-transfer coefficient h, Nusselt number Nu, pressure drop Δp, pumping power $P_{pump} = \Delta p \dot{V}$, heat transfer per unit pumping power Q/P_{pump}, and the selected performance factor or PEC.

For practical readiness, the relevant evidence is not only a higher Nu, but a sustained reduction in T_{max} and temperature non-uniformity within the allowable pressure-drop and pumping power limits of the target device. Flow maldistribution should also be quantified because manifold geometry and non-uniform inlet conditions can alter local mass flux, pressure drop, and thermal performance relative to idealized uniform-flow assumptions [135]. Therefore, system-level testing should report inlet/outlet temperature rise, local wall or surface temperature distribution, pressure distribution, and, where possible, channel-to-channel or region-to-region flow distribution.

Durability assessment should be coupled to this thermal-hydraulic validation. Lattice heat sinks should be exposed to thermal cycling, power cycling, sustained operation, pressure cycling for liquid-cooled systems, and vibration or shock conditions relevant to the application environment. TPMS and lattice structures are attractive because their continuous or periodic architectures can distribute mechanical loads, but practical deployment still requires evidence under thermal gradients, vibration, and shock [32,33]. For AM metallic lattices, this is especially important because residual stress, anisotropy, surface roughness, and node-level stress concentration can influence long-term structural reliability.

Adequate evidence of system-level readiness should therefore include: (i) stable R_{th}, T_{max}, $\Delta T_{surface}$, Δp, and P_{pump} before and after durability testing; (ii) no leakage, unacceptable blockage, or progressive increase in hydraulic resistance; (iii) no visible or CT-detected cracking, deformation, delamination, or severe fouling of the lattice core; and (iv) preservation of the thermal advantage over the baseline heat sink after cyclic or long-duration operation. Because acceptable limits depend on the device class, coolant, packaging technology, and reliability requirement, future studies should declare application-specific pass/fail criteria rather than reporting only component-level heat-transfer enhancement.

8.5. Design-Oriented Performance Maps

Future studies should provide integrated performance maps relating geometry, Reynolds number, and pumping power constraints within clearly defined normalization frameworks. Such maps should delineate: (i) operating regimes offering net system-level benefit, (ii) regions where hydraulic penalties dominate, and (iii) sensitivity to manufacturing tolerances and material limits. Embedding geometric descriptors, scaling conventions, and operating constraints into unified performance envelopes would enable application-specific selection rather than reliance on peak enhancement metrics. A transition toward normalization-consistent, manufacturable, and regime-aware design strategies is essential for advancing lattice heat sinks from exploratory geometric concepts to deployable thermal-management technologies in high-power and sustainable energy systems.

9. Conclusions

This review critically evaluated lattice-based heat sinks as volumetric thermal-management architectures for forced-convection cooling of high-power electronic systems. As power density increases across renewable-energy converters, electric mobility platforms, and energy-storage technologies, thermal management increasingly constrains efficiency, reliability, and lifetime. Lattice heat sinks offer a structurally distinct alterna-

tive to conventional fins by promoting three-dimensional flow–solid interaction within compact volumes.

Heat-transfer enhancement in lattice structures arises from boundary-layer disruption, wake-induced mixing, and distributed solid–fluid conduction pathways. These mechanisms can increase average Nusselt number and improve thermal uniformity. However, the same geometric features that intensify mixing also elevate flow tortuosity, frontal obstruction, and form drag, resulting in higher pressure-drop penalties. Performance is therefore governed by an inherent thermal-hydraulic trade-off rather than heat-transfer enhancement alone.

A central conclusion of this review is that lattice heat sinks do not universally outperform conventional cooling technologies. Their advantage is confined to specific combinations of porosity, ligament geometry, topology, Reynolds number, and confinement ratio in which heat-transfer gains offset hydraulic and pumping power costs. Many apparent contradictions in the literature stem from a combination of inconsistent geometric descriptors, Reynolds-number normalization, boundary-condition specification, manufacturing variability, and experimental uncertainty rather than from disagreement in underlying physics alone. Without unified scaling frameworks, transparent performance metrics, and documented experimental uncertainty, isolated reports of high Nusselt-number enhancement may misrepresent true system-level benefit.

Practical deployment further depends on manufacturability, material–geometry coupling, surface condition, durability under thermal cycling, and integration within constrained cooling loops. Additive manufacturing enables complex architectures, but scalability, repeatability, cost, and lifecycle energy considerations must be reconciled with thermo-fluid performance. Lattice heat sinks should therefore be evaluated as system-integrated thermal components rather than isolated geometric innovations.

Future progress requires unified geometric and normalization conventions, validation under realistic operating constraints, and design-oriented performance maps that balance heat-transfer enhancement against hydraulic and manufacturing costs. By shifting the objective from maximizing heat-transfer coefficients to achieving energy-efficient, manufacturable, and system-compatible solutions, research can transition lattice heat sinks from exploratory enhancement concepts toward deployable thermal-management technologies for high-power applications.

Author Contributions: Conceptualization, E.O., M.K. and W.L.; methodology, E.O. and M.K.; formal analysis, E.O. and W.L.; investigation, E.O. and W.L.; resources, W.L. and M.K.; data curation, E.O. and W.L.; writing—original draft preparation, E.O., M.K. and W.L.; supervision, W.L. and M.K. All authors have read and agreed to the published version of the manuscript.

Funding: This research received no external funding.

Data Availability Statement: The data presented in this study are available on request from the corresponding author.

Conflicts of Interest: The authors declare no conflicts of interest.

Appendix A. Mathematical Representation of Some Commonly Used TPMS Structures [33,41]

The commonly used TPMSs can be mathematically expressed with implicit level-set functions ($f(x, y, z) = C$), which define how the topology, periodicity, symmetry, connectivity, and curvature of the TPMS structure change based on the value of the representative level-set parameter (C) [33]. As C controls the surface location within the scalar field, changing the C value adjusts the effective thickness and relative density of the TPMS geometry without altering its topology [33]. $C = 0$ representing the baseline structure.

These functions are listed in Table A1 [32,33,41,143–146]. In these functions, the spatial frequencies ω_x, ω_y, and ω_z define the periodicity of the surface (unit-cell size) along the x, y, and z directions in the Cartesian coordinate system, respectively. The unit-cell size in each direction is determined by

$$L_i = 2\pi/\omega_i \quad \text{(A1)}$$

where i represents the x, y, and z directions, respectively. Variations in ω and C allow the generation of TPMS structures with uniform or graded relative density [41].

Table A1. Mathematical representations of some commonly used TPMS structures [32,33,41,143–146].

TPMS Structure	Implicit Level-Set Functions	Representative C Value
Gyroid	$f(x,y,z) = \sin(\omega_x x)\cos(\omega_y y) + \sin(\omega_z z)\cos(\omega_x x) + \sin(\omega_y y)\cos(\omega_z z) = C$	0.6
Fischer-Koch S (FKS)	$f(x,y,z) = \cos(2\omega_x x)\sin(\omega_y y)\cos(\omega_z z) + \cos(\omega_x x)\cos(2\omega_y y)\sin(\omega_z z) + \sin(\omega_x x)\cos(\omega_y y)\cos(2\omega_z z) = C$	0.375
Diamond	$f(x,y,z) = \cos(\omega_x x)\cos(\omega_y y)\cos(\omega_z z) - \sin(\omega_x x)\sin(\omega_y y)\sin(\omega_z z) = C$	0.45
Primitive	$f(x,y,z) = \cos(\omega_x x) + \cos(\omega_y y) + \cos(\omega_z z) = C$	0
Lidinold	$f(x,y,z) = \frac{1}{2}[\sin(2x)\cos(y)\sin(z) + \sin(2y)\cos(z)\sin(x) + \sin(2z)\cos(x)\sin(y)] - \frac{1}{2}[\cos(2x)\cos(y) + \cos(2y)\cos(2z) + \cos(2z)\cos(2x)] = C$	−0.15
IWP	$f(x,y,z) = 2[\cos(\omega_x x)\cos(\omega_y y) + \cos(\omega_y y)\cos(\omega_z z) + \cos(\omega_z z)\cos(\omega_x x)] - [\cos(2\omega_x x) + \cos(2\omega_y y) + \cos(2\omega_z z)] = C$	0
Neovius	$f(x,y,z) = 3[\cos(\omega_x x) + \cos(\omega_y y) + \cos(\omega_z z)] + 4\cos(\omega_x x)\cos(\omega_y y)\cos(\omega_z z) = C$	0
Schwarz P	$f(x,y,z) = \cos(x) + \cos(y) + \cos(z) = C$	0.67

References

1. Zhang, G.; Li, Z.; Zhang, B.; Halang, W.A. Power electronics converters: Past, present and future. *Renew. Sustain. Energy Rev.* **2018**, *81*, 2028–2044. [CrossRef]
2. Wileman, A.; Aslam, S.; Perinpanayagam, S. A road map for reliable power electronics for more electric aircraft. *Prog. Aerosp. Sci.* **2021**, *127*, 100739. [CrossRef]
3. Radomsky, L.; Keilmann, R.; Ferch, D.; Mallwitz, R. Challenges and opportunities in power electronics design for all-and hybrid-electric aircraft: A qualitative review and outlook. *CEAS Aeronaut. J.* **2024**, *15*, 751–764. [CrossRef]
4. Moreno, G.; Narumanchi, S.; Feng, X.; Anschel, P.; Myers, S.; Keller, P. Electric-drive vehicle power electronics thermal management: Current status, challenges, and future directions. *J. Electron. Packag.* **2022**, *144*, 011004.
5. Zhang, X.; Zhao, X.; Li, W.; Wang, Z.; Liao, A.; Song, Y.; Wang, Y.; Zhang, L. Ultra-thermostable embedded liquid cooling in SiC 3D packaging power modules of electric vehicles. *Energy Convers. Manag.* **2023**, *276*, 116499. [CrossRef]
6. Wang, W.; Niu, J.; Li, Y.Z.; Ren, K. Numerical study on heat transfer enhancement by spray-sublimation cooling with dry ice particles. *Appl. Therm. Eng.* **2022**, *214*, 118809. [CrossRef]
7. Mazaheri, N.; Mwesigye, A. On the thermal management of drive inverter modules: Energy-efficient heat sink design using topology optimization for cooling high heat flux power electronics. *Appl. Therm. Eng.* **2025**, *280*, 128398. [CrossRef]
8. Ji, B.; Song, X.; Sciberras, E.; Cao, W.; Hu, Y.; Pickert, V. Multiobjective design optimization of IGBT power modules considering power cycling and thermal cycling. *IEEE Trans. Power Electron.* **2014**, *30*, 2493–2504. [CrossRef]
9. Tan, L.; Liu, P.; She, C.; Xu, P.; Yan, L.; Quan, H. Heat dissipation characteristics of IGBT module based on flow-solid coupling. *Micromachines* **2022**, *13*, 554. [CrossRef] [PubMed]
10. Morel, C.; Morel, J.Y. Power semiconductor junction temperature and lifetime estimations: A review. *Energies* **2024**, *17*, 4589. [CrossRef]
11. Ahmad, F.; Vaccaro, L.; Nkembi, A.A.; Marchesoni, M.; Portesine, F.; Anyanwu, G. Junction Temperature and Failure Behavior of High-Power Press Pack vs. Module Diodes Under High Anomalous Surge Currents. *Electronics* **2025**, *15*, 121. [CrossRef]
12. Ozden, M.; Ozkan, G.; Rahman, S.I.; Buraimoh, E.; Timilsina, L.; Papari, B.; Edrington, C.S. Junction Temperature Prediction Model Development with Co-simulation. *e-Prime-Adv. Electr. Eng. Electron. Energy* **2025**, *12*, 101033. [CrossRef]
13. Kirchhofer, M.; Krieger, M.; Hofer, D. Experimental and numerical investigations of forced convection impingement heat transfer on plate-fin heat sinks using three different electronic cooling fans. *Appl. Therm. Eng.* **2025**, *258*, 124665. [CrossRef]
14. Ismail, M. Experimental and numerical analysis of heat sink using various patterns of cylindrical pin-fins. *Int. J. Thermofluids* **2024**, *23*, 100737. [CrossRef]
15. Wu, X.; Li, C.; Yang, J.; Liu, Y.; Han, X. Theoretical and experimental research on flow boiling heat transfer in microchannels for IGBT modules. *Int. J. Heat Mass Transf.* **2023**, *205*, 123900. [CrossRef]

16. Zhang, Z.; Zhang, G.; Zhang, Y.; Tian, M. Experimental study on the effect of hydraulic diameter on the flow boiling characteristics in microchannels. *Int. J. Heat Mass Transf.* **2025**, *241*, 126736. [CrossRef]
17. Parlak, F.; Sertkaya, A.A. Experimental investigation of forced convection heat transfer of heat exchangers with different pin geometries in in-line and staggered design. *Int. J. Heat Mass Transf.* **2024**, *231*, 125892. [CrossRef]
18. Kamma, P.; Loksupapaiboon, K.; Phromjan, J.; Promtong, M.; Suvanjumrat, C. Optimization of plate-fin heat sink configurations for enhanced thermal performance and manufacturability. *Case Stud. Therm. Eng.* **2025**, *73*, 106529. [CrossRef]
19. Kaur, I.; Aider, Y.; Nithyanandam, K.; Singh, P. Thermal-hydraulic performance of additively manufactured lattices for gas turbine blade trailing edge cooling. *Appl. Therm. Eng.* **2022**, *211*, 118461. [CrossRef]
20. Padrão, D.; Hancock, D.; Paterson, J.; Schoofs, F.; Tuck, C.; Maskery, I. New structure-performance relationships for surface-based lattice heat sinks. *Appl. Therm. Eng.* **2024**, *236*, 121572. [CrossRef]
21. Du Plessis, A.; Razavi, N.; Benedetti, M.; Murchio, S.; Leary, M.; Watson, M.; Bhate, D.; Berto, F. Properties and applications of additively manufactured metallic cellular materials: A review. *Prog. Mater. Sci.* **2022**, *125*, 100918. [CrossRef]
22. Dixit, T.; Nithiarasu, P.; Kumar, S. Numerical evaluation of additively manufactured lattice architectures for heat sink applications. *Int. J. Therm. Sci.* **2021**, *159*, 106607. [CrossRef]
23. Aider, Y.; Kaur, I.; Cho, H.; Singh, P. Periodic heat transfer characteristics of additively manufactured lattices. *Int. J. Heat Mass Transf.* **2022**, *189*, 122692. [CrossRef]
24. Park, K.; Kim, S.; Kim, J. Forced convection heat transfer in AlSi7Mg lattice structures fabricated by additive manufacturing. *Case Stud. Therm. Eng.* **2024**, *61*, 105006. [CrossRef]
25. Corbett, T.M.; Thole, K.A. Large eddy simulations of kagome and body centered cubic lattice cells. *Int. J. Heat Mass Transf.* **2024**, *218*, 124808. [CrossRef]
26. Kaur, I.; Singh, P. Numerical investigation on conjugate heat transfer in octet-shape-based single unit cell thick metal foam. *Int. Commun. Heat Mass Transf.* **2021**, *121*, 105090.
27. Vaglio, E.; Scalzo, F.; Scussolin, N.; Casarsa, L. Experimental investigation of heat transfer and pressure losses across additively manufactured Body Centered Cubic arrays: Effects of cell shape and array arrangement. *Appl. Therm. Eng.* **2025**, *280*, 128253. [CrossRef]
28. Batikh, A.; Fradin, J.P.; Castro Moreno, A. Computational and Experimental Investigation of Additively Manufactured Lattice Heat Sinks for Liquid-Cooling Railway Power Electronics. *Energies* **2025**, *18*, 3753. [CrossRef]
29. Alawwa, F.; Saeed, M.; Homsi, R.; Zhu, H.; Berrouk, A.S.; Khalil, M.; Xie, G.; Al Wahedi, Y. Thermohydraulic performance comparison of 3D printed circuit heatsinks with conventional integral fin heatsinks. *Appl. Therm. Eng.* **2023**, *226*, 120356. [CrossRef]
30. Sajjad, U.; Rehman, T.u.; Ali, M.; Park, C.W.; Yan, W.M. Manufacturing and potential applications of lattice structures in thermal systems: A comprehensive review of recent advances. *Int. J. Heat Mass Transf.* **2022**, *198*, 123352. [CrossRef]
31. Amara, K.; Saghir, M.Z.; Abdeljabar, R. Review of Triply Periodic Minimal Surface (TPMS) Structures for Cooling Heat Sinks. *Energies* **2025**, *18*, 4920. [CrossRef]
32. Wang, H.; Zhao, C.; Liu, W.; Liu, Z.; Bian, H.; Zhang, K. Advances in triply periodic minimal surface structures for thermal management systems: A comprehensive review. *Appl. Therm. Eng.* **2025**, *279*, 127481. [CrossRef]
33. Ifa, D.A.; Efa, D.A. TPMS-enabled architectures for heat dissipation in thermal systems: A review of current progress and future directions. *Int. J. Heat Mass Transf.* **2026**, *259*, 128401. [CrossRef]
34. Al-Safadi, M.; Ejaz, F.; Shuja, S.; Zubair, S.M. Quantitative Synthesis and Correlations of Heat Transfer and Friction Factor in Triply Periodic Minimal Surface (TPMS) Structures. *Results Eng.* **2026**, *29*, 109402. [CrossRef]
35. Kaur, I.; Singh, P. Critical evaluation of additively manufactured metal lattices for viability in advanced heat exchangers. *Int. J. Heat Mass Transf.* **2021**, *168*, 120858. [CrossRef]
36. Yan, H.; Wu, W.T.; Zhao, Z.; Feng, F. Review and comparison of turbulent convective heat transfer in state-of-the-art 3D truss periodic cellular structures. *Appl. Therm. Eng.* **2023**, *235*, 121450.
37. Dharmalingam, L.K.; Aute, V.; Ling, J. Review of triply periodic minimal surface (TPMS) based heat exchanger designs. In Proceedings of the International Refrigeration and Air Conditioning Conference, West Lafayette, IN, USA, 10–14 July 2022; p. 2393.
38. Yeranee, K.; Rao, Y. A Review of Recent Investigations on Flow and Heat Transfer Enhancement in Cooling Channels Embedded with Triply Periodic Minimal Surfaces (TPMS). *Energies* **2022**, *15*, 8994. [CrossRef]
39. Rashid, F.L.; Al Maimuri, N.M.; Al-Obaidi, M.A.; Eleiwi, M.A.; Ameen, A.; Ahmad, S.; Chibani, A.; Kezzar, M.; Agyekum, E.B. Enhancing heat transfer across applications with triply periodic minimal surface (TPMS) structures: A comprehensive review. *Chem. Eng. Process.-Process Intensif.* **2025**, *216*, 110460. [CrossRef]
40. Benedetti, M.; Du Plessis, A.; Ritchie, R.O.; Dallago, M.; Razavi, N.; Berto, F. Architected cellular materials: A review on their mechanical properties towards fatigue-tolerant design and fabrication. *Mater. Sci. Eng. R Rep.* **2021**, *144*, 100606. [CrossRef]

41. Hossain, M.S.; Hossain, M.M.; Nilufar, S. An Overview of Additive Manufacturing of Triply Periodic Minimal Surface (TPMS) Structures. *Polymers* **2025**, *17*, 3307. [CrossRef] [PubMed]
42. Chaudhari, A.; Ekade, P.; Krishnan, S. Experimental investigation of heat transfer and fluid flow in octet-truss lattice geometry. *Int. J. Therm. Sci.* **2019**, *143*, 64–75. [CrossRef]
43. Lorenzon, A.; Vaglio, E.; Casarsa, L.; Sortino, M. Experimental investigation of heat transfer and pressure losses across staggered Body Centered cubic arrays fabricated by Laser Powder Bed Fusion. *Appl. Therm. Eng.* **2023**, *227*, 120381. [CrossRef]
44. Liang, D.; Bai, W.; Chen, W.; Chyu, M.K. Investigating the effect of element shape of the face-centered cubic lattice structure on the flow and endwall heat transfer characteristics in a rectangular channel. *Int. J. Heat Mass Transf.* **2020**, *153*, 119579. [CrossRef]
45. Lorenzon, A.; Vaglio, E.; Casarsa, L.; Totis, G. Effects of different cross-sections of Body Centered Cubic cells on pressure drop and heat transfer of additively manufactured heat sinks. *Int. J. Heat Mass Transf.* **2024**, *222*, 125170. [CrossRef]
46. Liang, D.; Chen, W.; Ju, Y.; Chyu, M.K. Comparing endwall heat transfer among staggered pin fin, Kagome and body centered cubic arrays. *Appl. Therm. Eng.* **2021**, *185*, 116306. [CrossRef]
47. Liang, D.; He, G.; Chen, W.; Chen, Y.; Chyu, M.K. Fluid flow and heat transfer performance for micro-lattice structures fabricated by Selective Laser Melting. *Int. J. Therm. Sci.* **2022**, *172*, 107312. [CrossRef]
48. Iyer, J.; Moore, T.; Nguyen, D.; Roy, P.; Stolaroff, J. Heat transfer and pressure drop characteristics of heat exchangers based on triply periodic minimal and periodic nodal surfaces. *Appl. Therm. Eng.* **2022**, *209*, 118192. [CrossRef]
49. Khalil, M.; Ali, M.I.H.; Khan, K.A.; Al-Rub, R.A. Forced convection heat transfer in heat sinks with topologies based on triply periodic minimal surfaces. *Case Stud. Therm. Eng.* **2022**, *38*, 102313. [CrossRef]
50. Saghir, M.Z.; Kerme, E.D.; Hajialibabei, M.; Rasheed, H.; Welsford, C.; Al-Ketan, O. Study of the thermal and hydraulic performance of porous block versus gyroid structure: Experimental and numerical approaches. *Energies* **2024**, *17*, 861. [CrossRef]
51. Richard, S.; Tasso, D.; Rajana, M.; Saker, A.; Santos, A.R.; Makhloufi, C.; Meynet, N.; Hary, B.; Nardone, S.; Marino, G.; et al. Comparison of thermo-hydraulic performance among different 3D printed periodic open cellular structures. *Chem. Eng. J.* **2024**, *492*, 152005. [CrossRef]
52. Tang, W.; Zhou, H.; Zeng, Y.; Yan, M.; Jiang, C.; Yang, P.; Li, Q.; Li, Z.; Fu, J.; Huang, Y.; et al. Analysis on the convective heat transfer process and performance evaluation of Triply Periodic Minimal Surface (TPMS) based on Diamond, Gyroid and Iwp. *Int. J. Heat Mass Transf.* **2023**, *201*, 123642.
53. Ma, Y.; Yan, H.; Hooman, K.; Xie, G. Enhanced heat transfer in a pyramidal lattice sandwich panel by introducing pin-fins/protrusions/dimples. *Int. J. Therm. Sci.* **2020**, *156*, 106468. [CrossRef]
54. Oh, S.H.; Kim, J.E.; Jang, C.H.; Kim, J.; Park, C.Y.; Park, K. Multifunctional gradations of TPMS architected heat exchanger for enhancements in flow and heat exchange performances. *Sci. Rep.* **2025**, *15*, 19931. [CrossRef] [PubMed]
55. Orakwe, J.N.; Shahabad, S.I.; Ibhadode, O.; Bonakdar, A.; Toyserkani, E. An integration of topology optimization and conformal minimal surfaces for additively manufactured liquid-cooled heat sinks. *Addit. Manuf.* **2025**, *107*, 104814. [CrossRef]
56. Kong, D.; Jung, E.; Kim, Y.; Manepalli, V.V.; Rah, K.J.; Kim, H.S.; Hong, Y.; Choi, H.G.; Agonafer, D.; Lee, H. An additively manufactured manifold-microchannel heat sink for high-heat flux cooling. *Int. J. Mech. Sci.* **2023**, *248*, 108228. [CrossRef]
57. Yuan, L.; Zou, S.; Yang, Y.; Chen, S. Boundary-layer disruption and heat-transfer enhancement in convection turbulence by oscillating deformations of boundary. *Phys. Rev. Lett.* **2023**, *130*, 204001. [PubMed]
58. Arqam, M.; Raffa, L.S.; Ryall, M.; Islam, M.S.; Bennett, N.S. Numerical and experimental analysis of triply periodic minimal surface (TPMS)-based metal lattice heat sinks integrated with different phase change materials for enhanced thermal management of electronics. *J. Energy Storage* **2025**, *132*, 117784. [CrossRef]
59. Tian, R.; Meng, S.; Zheng, S.; Sun, X.; Wei, M. Thermo-hydraulic performance evaluation of lattice structures with triply periodic minimal surfaces for latent heat storage devices. *J. Energy Storage* **2024**, *102*, 114234. [CrossRef]
60. Barakat, A.; Sun, B. Enhanced convective heat transfer in new triply periodic minimal surface structures: Numerical and experimental investigation. *Int. J. Heat Mass Transf.* **2024**, *227*, 125538. [CrossRef]
61. Gao, C.; Xu, W.; Zhu, X.; Cui, J.; Luo, T.; Wang, D.; Sun, L.; Ling, W.; Li, X.; Zhou, W. Enhanced regenerative cooling performance with conformal TPMS channels. *Energy* **2025**, *322*, 135530. [CrossRef]
62. Ho, J.Y.; Leong, K.C.; Wong, T.N. Additively-manufactured metallic porous lattice heat exchangers for air-side heat transfer enhancement. *Int. J. Heat Mass Transf.* **2020**, *150*, 119262.
63. Soti, A.K.; Bhardwaj, R.; Sheridan, J. Flow-induced deformation of a flexible thin structure as manifestation of heat transfer enhancement. *Int. J. Heat Mass Transf.* **2015**, *84*, 1070–1081. [CrossRef]
64. Xu, H.; Yu, W.; Zhang, Y.; Ma, S.; Wu, Z.; Liu, X. Flow and heat transfer performance of bionic heat transfer structures with hybrid triply periodic minimal surfaces. *Appl. Energy* **2023**, *351*, 121847. [CrossRef]
65. Seetoh, I.; Markandan, K.; Lai, C.Q. Effect of reinforcement bending on the elastic properties of interpenetrating phase composites. *Mech. Mater.* **2019**, *136*, 103071. [CrossRef]
66. Kladovasilakis, N.; Tsongas, K.; Kostavelis, I.; Tzovaras, D.; Tzetzis, D. Effective mechanical properties of additive manufactured strut-lattice structures: Experimental and finite element study. *Adv. Eng. Mater.* **2022**, *24*, 2100879.

67. Shi, W.; Lin, Y.; Li, J.; Yang, M.; Liu, B. Optimization of mechanical properties of Ti-6Al-4V triply periodic minimal surface porous structures prepared by laser beam powder bed fusion technology based on orientation control. *Mater. Sci. Eng. A* **2024**, *894*, 146183.
68. Qian, M.; Li, J.; Xiang, Z.; Dong, Z.; Xiao, J.; Hu, X. Study on heat dissipation performance of a lattice porous structures under jet impingement cooling. *Case Stud. Therm. Eng.* **2023**, *49*, 103244. [CrossRef]
69. Caket, A.G.; Wang, C.; Nugroho, M.A.; Celik, H.; Mobedi, M. Recent studies on 3D lattice metal frame technique for enhancement of heat transfer: Discovering trends and reasons. *Renew. Sustain. Energy Rev.* **2022**, *167*, 112697. [CrossRef]
70. Xiao, Y.; Deng, H.; Yan, K.; Wang, J. Analysis of thermo-hydraulic performance in Gyroid-TPMS structures using Jacobian elliptic functions. *Energy Convers. Manag.* **2026**, *348*, 120707.
71. Wei, X.; Qian, Y.; Li, Y.; Gong, Z.; Yao, M.; Qian, D.; Hu, B. Investigation on the flow and heat transfer of a novel three-fluid heat exchanger based on TPMS. *Energy* **2025**, *314*, 134072. [CrossRef]
72. Yeranee, K.; Xu, C.; Rao, Y.; Zhang, Y. Experimental and numerical study of improving flow and heat transfer in a serpentine cooling channel with topology-optimized TPMS porous structures. *Int. J. Heat Mass Transf.* **2024**, *231*, 125873. [CrossRef]
73. Wagner, M.A.; Lumpe, T.S.; Chen, T.; Shea, K. Programmable, active lattice structures: Unifying stretch-dominated and bending-dominated topologies. *Extrem. Mech. Lett.* **2019**, *29*, 100461.
74. Son, K.N.; Weibel, J.A.; Kumaresan, V.; Garimella, S.V. Design of multifunctional lattice-frame materials for compact heat exchangers. *Int. J. Heat Mass Transf.* **2017**, *115*, 619–629. [CrossRef]
75. Deshpande, V.S.; Ashby, M.F.; Fleck, N.A. Foam topology: Bending versus stretching dominated architectures. *Acta Mater.* **2001**, *49*, 1035–1040. [CrossRef]
76. Pelanconi, M.; Zavattoni, S.; Cornolti, L.; Puragliesi, R.; Arrivabeni, E.; Ferrari, L.; Gianella, S.; Barbato, M.; Ortona, A. Application of ceramic lattice structures to design compact, high temperature heat exchangers: Material and architecture selection. *Materials* **2021**, *14*, 3225. [CrossRef] [PubMed]
77. Lee, H.; Lee, Y.J.; Kim, S.J. One-dimensional model of manifold microchannels for embedded cooling: Prediction of thermal performance and flow non-uniformity. *Int. Commun. Heat Mass Transf.* **2024**, *155*, 107498. [CrossRef]
78. Yan, H.; Zhang, Q.; Chen, W.; Xie, G.; Dang, J.; Lu, T.J. An X-lattice cored rectangular honeycomb with enhanced convective heat transfer performance. *Appl. Therm. Eng.* **2020**, *166*, 114687. [CrossRef]
79. Ekade, P.; Krishnan, S. Fluid flow and heat transfer characteristics of octet truss lattice geometry. *Int. J. Therm. Sci.* **2019**, *137*, 253–261. [CrossRef]
80. Kaur, I.; Singh, P. Flow and thermal transport through unit cell topologies of cubic and octahedron families. *Int. J. Heat Mass Transf.* **2020**, *158*, 119784. [CrossRef]
81. Kemerli, U.; Kahveci, K. Conjugate forced convective heat transfer in a sandwich panel with a Kagome truss core: The effects of strut length and diameter. *Appl. Therm. Eng.* **2020**, *167*, 114794. [CrossRef]
82. Kaur, I.; Singh, P. Conjugate heat transfer in lattice frame materials based on novel unit cell topologies. *Numer. Heat Transf. Part A Appl.* **2022**, *82*, 788–801. [CrossRef]
83. Shahrzadi, M.; Emami, M.D.; Akbarzadeh, A. Heat transfer in BCC lattice materials: Conduction, convection, and radiation. *Compos. Struct.* **2022**, *284*, 115159. [CrossRef]
84. Xu, J.; Gan, Y.; Zhang, D.; Li, X. Microscale heat transfer enhancement using thermal boundary layer redeveloping concept. *Int. J. Heat Mass Transf.* **2005**, *48*, 1662–1674. [CrossRef]
85. Ho, J.Y.; Leong, K.C.; Wong, T.N. Experimental and numerical investigation of forced convection heat transfer in porous lattice structures produced by selective laser melting. *Int. J. Therm. Sci.* **2019**, *137*, 276–287. [CrossRef]
86. Shi, X.; Yang, Z.; Chen, W.; Chyu, M.K. Investigation of the effect of lattice structure on the fluid flow and heat transfer of supercritical CO_2 in tubes. *Appl. Therm. Eng.* **2022**, *207*, 118132. [CrossRef]
87. Wang, X.; Wang, Y.; Xiao, X.; Chen, Z.; Kang, Y.; Lei, Y. Numerical study on heat transfer deterioration of supercritical CO_2 in lattice structure array channel. *Int. J. Heat Mass Transf.* **2024**, *227*, 125600. [CrossRef]
88. Ayadi, B.; Alrasheedi, N.H.; Mohsen, A.M.; Alizadeh, A.A.; Hussein, S.A.; Karouei, S.H.H.; Aich, W.; Hajlaoui, K. Performance augmentation of a double-coil heat exchanger: Analyzing the impact of radial fin count and diameter ratio. *Sci. Rep.* **2025**, *15*, 39877. [CrossRef] [PubMed]
89. Dadvand, A.; Hosseini, S.; Aghebatandish, S.; Khoo, B.C. Enhancement of heat and mass transfer in a microchannel via passive oscillation of a flexible vortex generator. *Chem. Eng. Sci.* **2019**, *207*, 556–580. [CrossRef]
90. Lee, S.Y.; Kim, K.W.; Kim, D.H.; Yang, M.S.; Kim, J.W.; Choi, G.; Lee, J.W.; Park, I.S. Optimization study on the uniform temperature of an additively manufactured cooler for a semiconductor heating device. *Appl. Therm. Eng.* **2023**, *225*, 120178. [CrossRef]
91. Aider, Y.; Singh, P. Experimental study on flow and thermal transport in additively manufactured architectured lattice frame with air and particles as convective agents. *J. Therm. Sci. Eng. Appl.* **2025**, *17*, 051006. [CrossRef]

92. Orville, T.; Tajwar, M.; Bihani, R.; Saha, P.; Hannan, M.A. Enhancing Thermal Efficiency in Power Electronics: A Review of Advanced Materials and Cooling Methods. *Thermo* **2025**, *5*, 30. [CrossRef]
93. Ali, D.; Sen, S. Finite element analysis of mechanical behavior, permeability and fluid induced wall shear stress of high porosity scaffolds with gyroid and lattice-based architectures. *J. Mech. Behav. Biomed. Mater.* **2017**, *75*, 262–270. [CrossRef] [PubMed]
94. Timercan, A.; Sheremetyev, V.; Brailovski, V. Mechanical properties and fluid permeability of gyroid and diamond lattice structures for intervertebral devices: Functional requirements and comparative analysis. *Sci. Technol. Adv. Mater.* **2021**, *22*, 285–300. [CrossRef] [PubMed]
95. Egan, P.F.; Gonella, V.C.; Engensperger, M.; Ferguson, S.J.; Shea, K. Computationally designed lattices with tuned properties for tissue engineering using 3D printing. *PLoS ONE* **2017**, *12*, e0182902. [CrossRef] [PubMed]
96. Rathore, S.S.; Mehta, B.; Kumar, P.; Asfer, M. Flow characterization in triply periodic minimal surface (TPMS)-based porous geometries: Part 1—Hydrodynamics. *Transp. Porous Media* **2023**, *146*, 669–701.
97. Cheng, Z.; Xu, R.; Jiang, P.X. Morphology, flow and heat transfer in triply periodic minimal surface based porous structures. *Int. J. Heat Mass Transf.* **2021**, *170*, 120902. [CrossRef]
98. Yun, S.; Kwon, J.; Lee, D.; Shin, H.H.; Kim, Y. Heat transfer and stress characteristics of additive manufactured FCCZ lattice channel using thermal fluid-structure interaction model. *Int. J. Heat Mass Transf.* **2020**, *149*, 119187. [CrossRef]
99. Narkhede, S.; Sur, A.; Tiwari, R. The effects of topological configuration and geometric parameters on heat transfer and fluid flow characteristics of lattice-based heat sinks. *Numer. Heat Transf. Part A Appl.* **2024**, *85*, 1481–1500.
100. Ahn, S.H.; Gwon, J.G.; Seo, Y.M.; Choi, H.K.; Park, Y.G. Effect of aspect ratio on heat transfer in lattice-structured channels for heat sinks. *J. Mech. Sci. Technol.* **2025**, *39*, 6381–6392. [CrossRef]
101. Abbasi, W.S.; Ehsan, M.; Rahman, H.; Uddin, Z.; Hassan, M.M.; Saleem, K. Analysis of the wake mechanism in external flow around tandem bluff bodies with different aspect ratios. *Front. Mech. Eng.* **2024**, *10*, 1341618. [CrossRef]
102. Attarzadeh, R.; Rovira, M.; Duwig, C. Design analysis of the "Schwartz D" based heat exchanger: A numerical study. *Int. J. Heat Mass Transf.* **2021**, *177*, 121415. [CrossRef]
103. Qian, C.; Wang, J.; Zhong, H.; Qiu, X.; Yu, B.; Shi, J.; Chen, J. Experimental investigation on heat transfer characteristics of copper heat exchangers based on triply periodic minimal surfaces (TPMS). *Int. Commun. Heat Mass Transf.* **2024**, *152*, 107292. [CrossRef]
104. Ferroni, C.; Franchi, F.S.; Ambrosetti, M.; Bracconi, M.; Groppi, G.; Maestri, M.; Tronconi, E. Numerical and experimental investigation of pressure drop in periodic open cellular structures for intensification of catalytic processes. *ACS Eng. Au* **2022**, *2*, 118–133. [CrossRef]
105. Shahid, M.U.; Shahid, M.N.; Khan, M.M.; Shahzad, M.W. Hydrothermal performance enhancement of microchannel heat sinks embedded with Schwarz-triply periodic minimal surface pin fins. *Int. Commun. Heat Mass Transf.* **2025**, *169*, 109628. [CrossRef]
106. Yahya, M.; Yahya, A.; Saghir, M. Experimental Measurement and Numerical Modelling of Solid Network-Based Schoen's I-Graph—Wrapped Package (I-WP) toward Cooling Heat Sink. *Therm. Sci. Appl.* **2025**, *1*, 3–20.
107. Bernardini, L.; Piacquadio, S.; Schröder, K.U.; Mameli, M.; Di Marco, P.; Filippeschi, S. Exploring the Impact of Unit Cell Size on Fluid Dynamics in Lattice Structures: Experimental and Numerical Insights. *Int. J. Thermofluids* **2025**, *31*, 101543. [CrossRef]
108. Parbat, S.; Min, Z.; Yang, L.; Chyu, M. Experimental and numerical analysis of additively manufactured inconel 718 coupons with lattice structure. *J. Turbomach.* **2020**, *142*, 061004. [CrossRef]
109. Ooi, A.; Lu, W.; Chan, L.; Cao, Y.; Leontini, J.; Skvortsov, A. Turbulent flow over a cylinder confined in a channel at Re = 3900. *Int. J. Heat Fluid Flow* **2022**, *96*, 108982. [CrossRef]
110. Mondal, R.; Alam, M.M. Blockage effect on wakes of various bluff bodies: A review of confined flow. *Ocean Eng.* **2023**, *286*, 115592. [CrossRef]
111. Kalogirou, I.D.; Romeos, A.; Giannadakis, A.; Mihalakakou, G.; Panidis, T. Vortex dynamics effects on the development of a confined turbulent wake. *Fluids* **2025**, *10*, 283. [CrossRef]
112. de Souza Mendes, P.R. A note on the Moody diagram. *Fluids* **2024**, *9*, 98. [CrossRef]
113. Webb, R.; Eckert, E. Application of rough surfaces to heat exchanger design. *Int. J. Heat Mass Transf.* **1972**, *15*, 1647–1658. [CrossRef]
114. Park, S.H.; Seo, D.H.; Jeong, J.H. Experimental and numerical analysis of thermal flow in open-cell porous metal during Darcy-Forchheimer transition regime. *Appl. Therm. Eng.* **2020**, *181*, 116029. [CrossRef]
115. Tang, W.; Zou, C.; Zhou, H.; Zhang, L.; Zeng, Y.; Sun, L.; Zhao, Y.; Yan, M.; Fu, J.; Hu, J.; et al. A novel convective heat transfer enhancement method based on precise control of Gyroid-type TPMS lattice structure. *Appl. Therm. Eng.* **2023**, *230*, 120797. [CrossRef]
116. Tang, W.; Guo, J.; Yang, F.; Zeng, L.; Wang, X.; Liu, W.; Zhang, J.; Zou, C.; Sun, L.; Zeng, Y.; et al. Performance analysis and optimization of the Gyroid-type triply periodic minimal surface heat sink incorporated with fin structures. *Appl. Therm. Eng.* **2024**, *255*, 123950. [CrossRef]
117. Chen, L.Y.; Liang, S.X.; Liu, Y.; Zhang, L.C. Additive manufacturing of metallic lattice structures: Unconstrained design, accurate fabrication, fascinated performances, and challenges. *Mater. Sci. Eng. R Rep.* **2021**, *146*, 100648. [CrossRef]

118. Jost, E.W.; Pegues, J.; Moore, D.; Saldaña, C. Process-structure-property relationships of laser powder bed fusion lattice structures. *J. Manuf. Sci. Eng.* **2023**, *145*, 091007. [CrossRef]
119. Metelkova, J.; Vanmunster, L.; Haitjema, H.; Van Hooreweder, B. Texture of inclined up-facing surfaces in laser powder bed fusion of metals. *Addit. Manuf.* **2021**, *42*, 101970. [CrossRef]
120. Rott, S.; Ladewig, A.; Friedberger, K.; Casper, J.; Full, M.; Schleifenbaum, J.H. Surface roughness in laser powder bed fusion–Interdependency of surface orientation and laser incidence. *Addit. Manuf.* **2020**, *36*, 101437.
121. Wu, Z.; Narra, S.P.; Rollett, A. Exploring the fabrication limits of thin-wall structures in a laser powder bed fusion process. *Int. J. Adv. Manuf. Technol.* **2020**, *110*, 191–207. [CrossRef]
122. Kaur, I.; Singh, P. Effects of inherent surface roughness of additively manufactured lattice frame material on flow and thermal transport. *Int. J. Heat Mass Transf.* **2023**, *209*, 124077. [CrossRef]
123. Wildgoose, A.J.; Thole, K.A.; Tuneskog, E.; Wang, L. Roughness related to cooling performance of channels made through additive manufacturing. In *Turbo Expo: Power for Land, Sea, and Air*; American Society of Mechanical Engineers: New York, NY, USA, 2023; Volume 87011, p. V07BT13A014.
124. Vafadar, A.; Guzzomi, F.; Hayward, K. Experimental investigation and comparison of the thermal performance of additively and conventionally manufactured heat exchangers. *Metals* **2021**, *11*, 574. [CrossRef]
125. Bichnevicius, M.; Saltzman, D.; Lynch, S. Comparison of louvered plate-fin heat exchangers made via additive manufacturing. In *ASME International Mechanical Engineering Congress and Exposition*; American Society of Mechanical Engineers: New York, NY, USA, 2018; Volume 52019, p. V002T02A061.
126. Zhou, Y.; Shen, S.; Liu, T.; Li, P.; Duan, F. Effective heat conduction evaluation of lattice structures from selective laser melting printing. *Int. J. Heat Mass Transf.* **2024**, *218*, 124790.
127. Aider, Y.; Kaur, I.; Mujahid, S.; Paudel, Y.; Rhee, H.; Singh, P. Enhanced Heat Transfer Through Additively Manufactured Architectured Lattice Frame Materials in SS316L and Ti-6Al-4V. In *Heat Transfer Summer Conference*; American Society of Mechanical Engineers: New York, NY, USA, 2024; Volume 87905, p. V001T05A005.
128. Wei, B.; Luo, W.; Du, J.; Ding, Y.; Guo, Y.; Zhu, G.; Zhu, Y.; Li, B. Thermal interface materials: From fundamental research to applications. *SusMat* **2024**, *4*, e239. [CrossRef]
129. Sun, S.; Rankouhi, B.; Thoma, D.J.; Cheadle, M.J.; Maples, G.D.; Anderson, M.H.; Nellis, G.; Qian, X. Topology optimization, additive manufacturing and thermohydraulic testing of heat sinks. *Int. J. Heat Mass Transf.* **2024**, *224*, 125281. [CrossRef]
130. Nafis, B.M.; Whitt, R.; Iradukunda, A.C.; Huitink, D. Additive manufacturing for enhancing thermal dissipation in heat sink implementation: A review. *Heat Transf. Eng.* **2021**, *42*, 967–984.
131. Liao, J.; Cooper, D.R. The environmental impacts of metal powder bed additive manufacturing. *J. Manuf. Sci. Eng.* **2021**, *143*, 030801.
132. Torres-Carrillo, S.; Siller, H.R.; Vila, C.; López, C.; Rodríguez, C.A. Environmental analysis of selective laser melting in the manufacturing of aeronautical turbine blades. *J. Clean. Prod.* **2020**, *246*, 119068. [CrossRef]
133. Yuruker, S.U.; Mandel, R.K.; McCluskey, P.; Ohadi, M.M. Air cooling of power electronics through vertically enhanced manifold microchannel systems (VEMMS). *J. Heat Transf.* **2021**, *143*, 101501. [CrossRef]
134. Zhu, Q.; Pishahang, M.; Bichnevicius, M.; Amy, C.; Caccia, M.; Sandhage, K.H.; Henry, A. The importance of maldistribution matching for thermal performance of compact heat exchangers. *Appl. Energy* **2022**, *324*, 119576. [CrossRef]
135. Guo, X.; Li, Z.; Zhai, Y.; Wang, H. Flow maldistribution and its effect on the thermal performance of miniaturized devices: A perspective from thermal boundary condition. *Energy Rev.* **2024**, *3*, 100098. [CrossRef]
136. Zhang, K.; Li, M.J.; Liu, H.; Xiong, J.G.; He, Y.L. A general and rapid method to evaluate the effect of flow maldistribution on the performance of heat exchangers. *Int. J. Therm. Sci.* **2021**, *170*, 107152. [CrossRef]
137. Huangfu, B.; Liu, Y.; Liu, X.; Wu, X.; Bai, H. Anisotropy of additively manufactured metallic materials. *Materials* **2024**, *17*, 3653. [CrossRef] [PubMed]
138. Qin, S.; Herzog, S.; Kaletsch, A.; Broeckmann, C. A microstructural modification strategy to improve thermal conductivity of tool steels produced by laser powder bed fusion. *Mater. Charact.* **2024**, *211*, 113917. [CrossRef]
139. Liu, H.; Cai, G.; Peng, K.; Jin, H.; Alexander, A. Thermal Behavior and Mechanical Properties of Different Lattice Structures Fabricated Using Selective Laser Melting. *Materials* **2024**, *17*, 5603. [CrossRef] [PubMed]
140. Pelegatti, M.; Scalzo, F.; Sordetti, F.; Vaglio, E.; Magnan, M.; Totis, G.; Sortino, M.; Benasciutti, D.; Lanzutti, A.; De Bona, F.; et al. Low cycle fatigue behaviour of cellular materials: Experimental comparative study of strut-based and gyroid structures made of additively manufactured 316L steel. *Int. J. Fatigue* **2024**, *178*, 108024. [CrossRef]
141. Collini, F.; Meneghetti, G. Towards a fracture mechanics-based fatigue assessment of lattice structures obtained from additive manufacturing of metallic powders. *Mater. Des.* **2024**, *244*, 113077. [CrossRef]
142. Muslu, A.M.; Joshi, Y. Unlocking the Potential of Integrated Cooling and Power Delivery in Multi-chip Power Electronics Packages with Triply Periodic Minimal Surfaces (TPMS). *Int. J. Heat Mass Transf.* **2026**, *255*, 127866.

143. Yoo, D.J. Computer-aided porous scaffold design for tissue engineering using triply periodic minimal surfaces. *Int. J. Precis. Eng. Manuf.* **2011**, *12*, 61–71. [CrossRef]
144. Karakoç, A. RegionTPMS — Region based triply periodic minimal surfaces (TPMS) for 3-D printed multiphase bone scaffolds with exact porosity values. *SoftwareX* **2021**, *16*, 100835. [CrossRef]
145. Chris-Amadin, H.; Ibhadode, O. LattGen: A TPMS lattice generation tool. *Softw. Impacts* **2024**, *21*, 100665. [CrossRef]
146. Malekshahi, A.; Salami, S.J.; Geramizadeh, H.; Dariushi, S. A novel combined tubular 3D-printed lattice structures with coupling effects for enhancing energy absorption. *Results Eng.* **2025**, *26*, 105350. [CrossRef]

Disclaimer/Publisher's Note: The statements, opinions and data contained in all publications are solely those of the individual author(s) and contributor(s) and not of MDPI and/or the editor(s). MDPI and/or the editor(s) disclaim responsibility for any injury to people or property resulting from any ideas, methods, instructions or products referred to in the content.